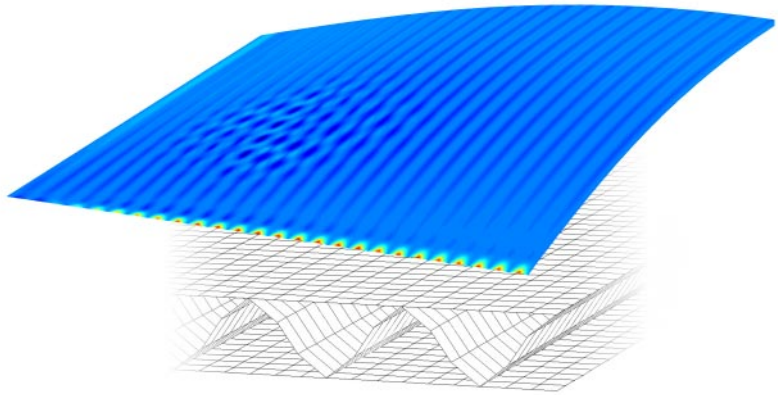




**LUND**  
UNIVERSITY



# **STABILITY AND COLLAPSE OF CORRUGATED BOARD; Numerical and Experimental Analysis**

ANDREAS ALLANSSON and BJÖRN SVÄRD

Structural  
Mechanics

*Master's Dissertation*

Structural Mechanics

ISRN LUTVDG/TVSM--01/5102--SE (1-74)

ISSN 0281-6679

STABILITY AND COLLAPSE OF  
CORRUGATED BOARD;  
Numerical and Experimental Analysis

Master's Dissertation by  
ANDREAS ALLANSSON and BJÖRN SVÄRD

Supervisors:

ULF NYMAN, PER JOHAN GUSTAFSSON and  
LILIANA BELDIE, Div. of Structural Mechanics  
TOMAS NORDSTRAND, SCA Research, Sundsvall

Copyright © 2001 by Structural Mechanics, LTH, Sweden.  
Printed by KFS i Lund AB, Lund, Sweden, January 2001.

For information, address:  
Division of Structural Mechanics, LTH, Lund University, Box 118, SE-221 00 Lund, Sweden.  
Homepage: <http://www.byggmek.lth.se>

# Abstract

This master's thesis describes nonlinear finite element analysis and experimental verification tests of a corrugated board panel when loaded in-plane. Detailed modelling of a panel, where both the liner and fluting is represented in detail, is compared to simplified shell modelling with a solid core and to experimental tests. In the experimental tests, Stereoscopic Digital Speckle Photography is used to obtain the in-plane as well as the out-of-plane displacements. The analyses shows that a local phenomenon as buckling of the liner between the corrugations is important for the global load-displacement response. It is also shown that it is possible to predict the load carrying capacity with a simple composite model if a failure criterion that considers both material and structural failure is used.

**Keywords:** FEM, finite element analysis, corrugated board, buckling, postbuckling, tests, strength, collapse, packages

---

The cover picture illustrates the local deformation pattern of the facing and the numerical model used in the computer simulations.



# Preface

This report is the outcome of our master's dissertation work. It was made in the field of structural mechanics. The work was carried out during the summer and autumn of year 2000 at the Division of Structural Mechanics, Lund University, excepts for the experimental tests that were performed at SCA Research in Sundsvall.

We would like to express our gratitude to our supervisors, Lic. Eng. Ulf Nyman and Doc. Per Johan Gustafsson at the Division of Structural Mechanics for their invaluable guidance and support during the course of the work. We would also like to thank M.Sc. Tomas Nordstrand and B.Sc. Rickard Boman at SCA Research for their help with the experimental tests. We are also grateful to all the people at Structural Mechanics for being there when we needed it.

Finally, we would like to thank Linda and Charlotta for their love and support.

Lund, January 2001

Andreas Allansson      Björn Svärd



# Summary

The purpose of this master's thesis was to perform a detailed finite element analysis of a 400x400 mm corrugated board panel. Previous work in this area has mostly been concerned with simplified composite models where the corrugated layer is replaced by a solid core. In this work a detailed finite element analysis (FEA) is performed, where the veritable geometry is modelled, i.e. the corrugated fluting is modelled by structural elements. The purpose is to study the influence of the local buckling of the facings on the global performance of the panel, see figure 1.

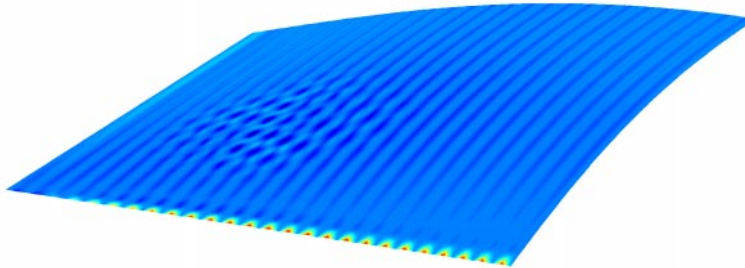


Figure 1: The local buckling pattern and shape of liner 200 WTK.

The results from the detailed FEA are compared with results from a simplified model and with results from experimental tests. In order to examine the effects of local buckling on the board's total load carrying capacity, a material as well as a structural failure criterion, is considered.

It is shown that a good agreement between the load-displacement paths of the FEA and the experimental tests can be achieved even when a linear-elastic orthotropic material model is used. In the detailed analysis, the collapse load for both structural and material failure is close to the mean collapse load from the experimental tests, 1677 N. The collapse loads are 5.8 % and 2.8 % lower for structural and material failure respec-

tively. Concerning the simplified analysis, the collapse load predicted by material failure will overestimate the strength with 16.3 %. For structural failure, the collapse load is 3.2 % larger than the collapse load from the tests.

Computational analyses were also made for various out-of-plane shear stiffnesses of the papers. These analyses indicated a significant effect of these shear stiffnesses on the load bearing capacity of the panels.

# Contents

<b>1</b>	<b>Introduction</b>	<b>1</b>
1.1	Background . . . . .	1
1.2	Aim and scope of the thesis . . . . .	1
1.3	Formulation of the problem . . . . .	2
1.4	Procedure of solving the problem . . . . .	2
<b>2</b>	<b>Corrugated board</b>	<b>5</b>
2.1	History . . . . .	5
2.2	Manufacturing . . . . .	5
2.3	Today's field of application . . . . .	7
2.4	Future development . . . . .	8
<b>3</b>	<b>Theory</b>	<b>9</b>
3.1	The principles of a sandwich structure . . . . .	9
3.2	Constitutive properties of paper . . . . .	9
3.3	Buckling of a structural core sandwich . . . . .	11
3.4	Eigenvalue buckling prediction . . . . .	12
3.5	Nonlinear postbuckling analysis . . . . .	13
3.6	Damped postbuckling . . . . .	14
3.7	Failure criteria of the facings . . . . .	15
<b>4</b>	<b>Finite element analysis</b>	<b>19</b>

4.1	Detailed model . . . . .	19
4.1.1	Geometry modelling . . . . .	19
4.1.2	Material modelling . . . . .	20
4.1.3	Finite element mesh . . . . .	22
4.1.4	Boundary conditions . . . . .	24
4.2	Buckling . . . . .	26
4.3	Postbuckling . . . . .	26
4.4	Simplified model . . . . .	27
4.5	Matlab post-processor . . . . .	29
4.6	Results . . . . .	32
4.6.1	Detailed model . . . . .	32
4.6.2	Simplified model . . . . .	39
<b>5</b>	<b>Experimental study</b>	<b>43</b>
5.1	Equipment and set-up . . . . .	43
5.1.1	MTS test frame . . . . .	43
5.1.2	Digital Speckle Photography . . . . .	45
5.2	Test procedure . . . . .	46
5.3	Results . . . . .	49
<b>6</b>	<b>Comparison of results</b>	<b>53</b>
6.1	Load-displacement response . . . . .	53
6.2	Stress development . . . . .	55
6.3	Failure criteria . . . . .	57
<b>7</b>	<b>Concluding remarks</b>	<b>61</b>
7.1	Conclusions . . . . .	61
7.2	Future work and improvements . . . . .	61

# Chapter 1

## Introduction

### 1.1 Background

Corrugated board is used mostly as a packaging material, e.g. in storage boxes. The most important loading case for this type of application is compressive loading, e.g. from boxes standing on top of each other. When the loading of a board becomes large, the board will collapse, either by structural or by material failure. Before the collapse of the board, local buckling between the corrugations may occur, which might have a significant effect on the board's total load carrying capacity.

As the field of application for corrugated board is widened, the need for optimization of the material properties increases. In order to optimize the material properties and the geometrical shape for different purposes, design curves are required. Such design curves can be created by performing several numerical analyses, e.g. finite element analyses (FEA), on the same model with different material-, geometry- and load-parameter combinations. This use of FEA is only justified if it is shown that the response of the model is in agreement with the actual response.

### 1.2 Aim and scope of the thesis

The purpose of this master thesis is to perform a detailed finite element analysis of a corrugated board panel when loaded in-plane. In the detailed analysis, the veritable geometry is modelled, i.e. both the liner and

the fluting is represented by their actual plane and corrugated geometry, respectively. The results from the FEA are to be compared with those from an experimental study, therefore the geometrical and material properties of the FE model must agree with the test panel. In the analysis, both local and global stability is to be considered, especially the effects of local buckling on the board's total load carrying capacity. In addition to the detailed model is a simplified model analysed, where the corrugated layer is replaced by a solid core. The solid core stiffness properties in this model are determined as effective stiffnesses, equivalent to those of the corrugated medium. The purpose of this analysis is to verify if a simplified composite stress analysis is possible in order to accurately simulate the collapse of the board. This thesis is also meant to be the base for a parametric study at SCA Research, in order to obtain design curves to optimize the material properties. Since the material represents approximately half of the product cost there is a lot of money to save even in a small reduction of the material consumption.

The size of the modelled panel is limited by computer resources, due to the large amount of degrees of freedom. The material behaviour is approximated to be linear-elastic by two reasons. One is that currently, no accurate nonlinear material model for paper is available and, secondly, the computation time would most probably increase very much if, in addition to the nonlinear geometry modelling, also nonlinear material modelling is included.

### **1.3 Formulation of the problem**

When the board is loaded in-plane it will have a very complex nonlinear load-deformation path and may fail by different failure modes. In order to capture this nonlinear response in the FEA an incremental technique is required.

### **1.4 Procedure of solving the problem**

The commercial general purpose FE-program Abaqus and the commercial mathematics and matrix program Matlab were used in the computational work. The different steps in solving the present task can be

summarized as:

- Create the detailed model and its corresponding Abaqus input file using Matlab for easy change of model parameters. The composite model is generated solely by Abaqus.
- Perform a convergence study on a local structural part, using eigenvalue buckling prediction, to decide which element type and mesh to use.
- Estimate the elastic buckling load of the board and calculate the first buckling mode by eigenvalue extraction. This is done for both the detailed model and the composite model. The modes are then used as imperfections of the panel geometry in the nonlinear analyses.
- A nonlinear post buckling analysis is performed, for the two models. From the analyses, load-deformation paths are obtained and it is possible to visualize the influence of local buckling and how this effects the total load carrying capacity of the corrugated board panel.
- Evaluate the computed stresses by means of a material failure criteria to get an estimation of the instant of material failure. In addition, the stress state at collapse is compared with a structural (local buckling) failure criteria.
- Finally, an experimental study is performed in order to verify and evaluate the theoretical models.



# Chapter 2

## Corrugated board

### 2.1 History

In 1856 two Englishmen, Healy and Allen, received the first patent on corrugated paper. With a simple hand-driven machine they produced a corrugated paper that was used as a lining in hats. The American Albert L Jones attached a plane sheet to the corrugated paper and patented the technique in which heat was used to corrugate paper in 1871. This product was used to protect fragile goods as bottles. Then in 1874 the American Oliver Long patented the concept of strengthening the corrugated paper by adding another facing. The first Swedish manufacturing of corrugated board was started in Malmö by Carl Th Norén in 1905. The improvement of the machines made it possible to produce corrugated board of higher quality and in the 1920's the boxes made of corrugated board started to compete with the ones made of wood. [1, 2]

### 2.2 Manufacturing

Corrugated board consists of one or several layers of corrugated paper which is glued on or in between plane sheets of paper, see figure 2.1.

The manufacturing process can roughly be divided into two parts. The wet part, where the fluting is corrugated between two rolls and then glued onto the liner, see figure 2.2, and the dry part, where heat is applied to dry the corrugated board. A problem in the manufacturing of corrugated

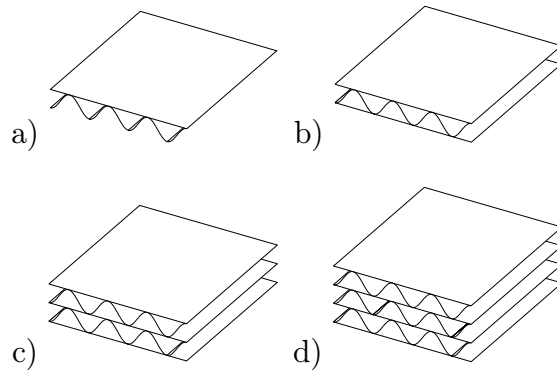


Figure 2.1: Different types of corrugated board: a) Single face. b) Single wall. c) Double wall. d) Triple wall.

board is when the moisture contents in the different layers are out of balance. Then the corrugated board can deform in a buckling shape or as a dip in the facings between the corrugations. These phenomena are called *warp* and *washboard* respectively [3].

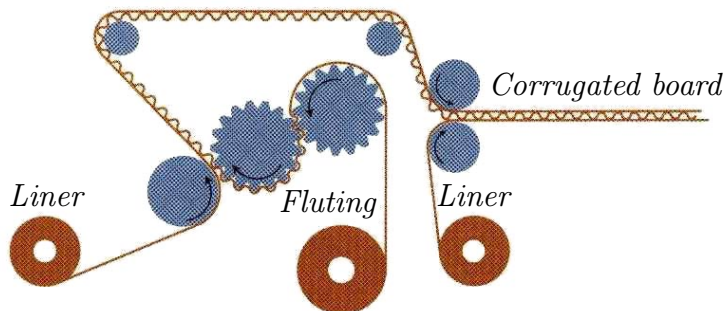


Figure 2.2: The manufacturing of a single wall corrugated board.

As well as there are different types of panels there are different flute profiles, see table 2.1<sup>1</sup>.

Corrugated board is often considered to be the packaging material of the

<sup>1</sup>The inconsequence in profile notation, for profiles B and C, in regard to the height, is due to the order in which the two profiles were invented.

Table 2.1: Different flute profiles.

Flute profile	Height (mm)	Number of corrugations/m
A	4.8	110
B	2.4	150
C	3.6	130
E	1.2	290
F	0.7	350
G & N	0.5	550

future. There are many advantages and very few disadvantages. Some of them are:

- + Low weight. Saves money when transporting.
- + Can be entirely customised for the purpose.
- + It is strong and stiff compared to its weight.
- + Easy to handle.
- + Easy to print.
- + Fully recyclable. In Sweden 98 % of the produced corrugated board is recycled [4].
- Very sensitive to humidity.

## 2.3 Today's field of application

Corrugated board is mainly used in packaging and can be customised entirely for its purpose. If a moisture-repellent membrane is applied on the surface the box can contain wet products, see figure 2.3. In the fish industries this is useful, because the box is only used once and does not need to be washed or transported back after delivery. Instead, the box can be recycled immediately after it has served its purpose. An example of a new type of application is pallets, on which goods can be stapled.



Figure 2.3: A box made of corrugated board containing wet products, in this case fish.

## 2.4 Future development

The development of flute profiles with very small wave-heights, micro-flute, has made corrugated board to a strong competitor to cardboard. A new product area, is e.g. consumer packages. Here the high stiffness of the thin corrugated board type, in comparison with the small amount of material used, makes it a favourable alternative to cardboard.

# Chapter 3

## Theory

This chapter describes theory used in chapter 4 and should be considered only as a brief introduction.

### 3.1 The principles of a sandwich structure

The studied corrugated board consists of a core, the fluting, and of two facings, the liners. As for a typical sandwich material, the purpose of the facings are to carry normal stresses resulting from in-plane deformation and curvature of the board. The purpose of the core is to carry shear stresses and to keep the facings apart. Since the core is supposed to stabilize the facings it must possess sufficient rigidity against deformation in planes normal to the facings. It is these two properties that give rise to the outstanding strength and stiffness characteristics, compared to the low weight, of a sandwich structure. The distance between the facings also affects the stiffness properties of the sandwich. The larger distance, the stiffer the composite will be in bending. The layers can be very weak when separated, but together they create a stiff composite.

### 3.2 Constitutive properties of paper

Since paper is made of oriented wood fibres the stiffness and strength properties are anisotropic. Commonly the fibre orientation is approxi-

mately symmetric. This means that the stiffness properties can be assumed to be orthotropic, i.e. three symmetry planes for the elastic properties can be found. Therefore, the constitutive relation, the relation between stresses and strains, for paper is assumed to be:

$$\begin{bmatrix} \epsilon_x \\ \epsilon_y \\ \epsilon_z \\ \gamma_{xy} \\ \gamma_{xz} \\ \gamma_{yz} \end{bmatrix} = \begin{bmatrix} \frac{1}{E_x} & \frac{-\nu_{yx}}{E_y} & \frac{-\nu_{zx}}{E_z} & 0 & 0 & 0 \\ \frac{-\nu_{xy}}{E_x} & \frac{1}{E_y} & \frac{-\nu_{zy}}{E_z} & 0 & 0 & 0 \\ \frac{-\nu_{xz}}{E_x} & \frac{-\nu_{yz}}{E_y} & \frac{1}{E_z} & 0 & 0 & 0 \\ 0 & 0 & 0 & \frac{1}{G_{xy}} & 0 & 0 \\ 0 & 0 & 0 & 0 & \frac{1}{G_{xz}} & 0 \\ 0 & 0 & 0 & 0 & 0 & \frac{1}{G_{yz}} \end{bmatrix} \begin{bmatrix} \sigma_x \\ \sigma_y \\ \sigma_z \\ \tau_{xy} \\ \tau_{xz} \\ \tau_{yz} \end{bmatrix} \quad (3.1)$$

Symmetry leads to

$$\frac{\nu_{xy}}{E_x} = \frac{\nu_{yx}}{E_y}, \quad \frac{\nu_{xz}}{E_x} = \frac{\nu_{zx}}{E_z}, \quad \frac{\nu_{yz}}{E_y} = \frac{\nu_{zy}}{E_z} \quad (3.2)$$

Now only nine unknown parameters remain,  $E_x$ ,  $E_y$ ,  $E_z$ ,  $\nu_{xy}$ ,  $\nu_{xz}$ ,  $\nu_{yz}$ ,  $G_{xy}$ ,  $G_{xz}$ ,  $G_{yz}$ . Generally, these parameters have to be measured. However, some of the parameters are not straightforward to measure, due to the small dimension in the thickness direction of paper. The in-plane properties,  $E_x$  and  $E_y$ , can fairly easy be obtained by standard tests, e.g. stress-strain curves. For the rest of the parameters, estimations can be used to obtain approximate values.

According to [5] is

$$E_z = \frac{E_x}{200} \quad (3.3)$$

a good approximation for the Young's modulus in the out-of-plane direction. The shear moduli are approximated according to [6, 7] with

$$\begin{aligned} G_{xy} &= 0.387\sqrt{E_x E_y} \\ G_{xz} &= E_x/55 \\ G_{yz} &= E_y/35 \end{aligned} \quad (3.4)$$

The values of  $\nu_{xy}$ ,  $\nu_{xz}$  and  $\nu_{yz}$  are set according to [14]. In addition to the approximations in (3.4), are values of  $G_{xz}$  and  $G_{yz}$ , suggested in [14], also used in the analyses. A trial and error procedure has also been performed, in which different values of  $G_{xz}$  and  $G_{yz}$  have been tested, in order to get results that are as similar as possible to the tests.

### 3.3 Buckling of a structural core sandwich

A slender structure carries its load by axial or membrane action, see figure 3.1, rather than by bending action. The out-of-plane deformation is usually very small at load levels below the critical buckling load. When the critical load is reached, the structure often deforms rapidly and the in-plane stiffness decreases.

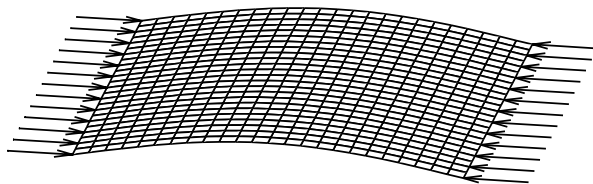


Figure 3.1: Plate loaded in-plane.

Corrugated board can buckle in two different ways, globally or locally. Local buckling occurs when the board facings buckle between the corrugations and global is when the entire board buckles, see figure 3.2. The theory is the same in the two cases, it is only the geometry of the structure and the boundary and loading conditions that are different.

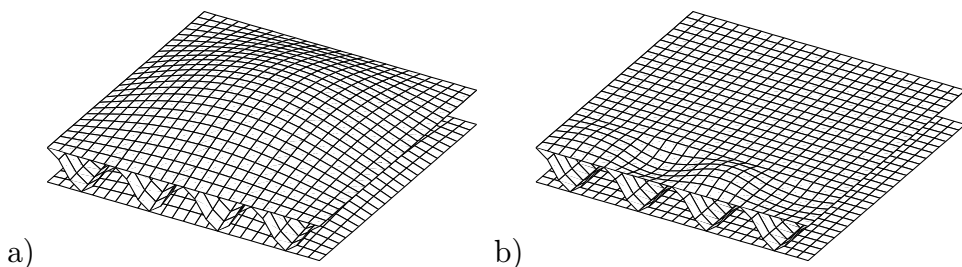


Figure 3.2: a) Global and b) local buckling of a corrugated board.

### 3.4 Eigenvalue buckling prediction

Eigenvalue buckling analysis is often used to predict the critical buckling load and failure mode of a structure. In the general eigenvalue buckling problem the critical load is given when the stiffness matrix becomes singular, so that (3.5) has nontrivial solutions.

$$\mathbf{K}\boldsymbol{\nu} = 0 \quad (3.5)$$

$\mathbf{K}$  is the tangent stiffness matrix when the loads are applied and  $\boldsymbol{\nu}$  are the nontrivial displacement solutions. In Abaqus [8], an incremental technique is used in the eigenvalue buckling problem:

$$(\mathbf{K}_0 + \lambda_i \mathbf{K}_\Delta) \boldsymbol{\nu}_i = 0 \quad (3.6)$$

$\mathbf{K}_0$  is the initial stiffness matrix,  $\mathbf{K}_\Delta$  is the differential stiffness matrix due to the applied load,  $\lambda_i$  are the eigenvalues and  $\boldsymbol{\nu}_i$  are the corresponding eigenvectors, i.e. the shape of the buckling modes. The critical buckling load is obtained by multiplying the applied load with the lowest eigenvalue,  $\lambda_1$ . The eigenvectors  $\boldsymbol{\nu}_i$  are normalized so that the maximum displacement component has a magnitude of 1.0. The direction, i.e. the sign, of the buckling displacement is not found by the eigenvalue analysis. In order to stipulate which direction to use in the postbuckling analysis, there are two possibilities. One is to perform a nonlinear postbuckling analysis on a geometrically perfect panel and from this get the correct direction. This is possible if the panel consists of a non-symmetric lay-up of individual layers, i.e. a coupling exists between membrane and bending action. The other is to study in which direction a real panel buckles, when exposed to a compression test. The results from the two possibilities, might not be similar if the real panel have an imperfection large enough to affect which buckling mode the panel gets when loaded. They will also differ if the panel is forced to buckle in a certain mode by the testing equipment, e.g. by asymmetric loading conditions.

### 3.5 Nonlinear postbuckling analysis

The nonlinear geometry response due to large deformations, requires an incremental technique to capture the complex load and displacement performance during the analysis, see figure 3.3. In a displacement controlled analysis, the displacement,  $\Delta \mathbf{a}^1$ , is prescribed in the first iteration in each increment and then the internal forces,  $\mathbf{f}_{int}$ , are calculated at this new load level. The difference between the total applied load,  $\mathbf{P}$ , and the internal forces are the out-of-balance forces,  $\boldsymbol{\psi}$ , for this iteration. Then the largest out-of-balance force at any degree of freedom is compared to the out-of-balance tolerance and if it is less then the structure is in equilibrium. If not, then these out-of-balance forces are the load in the following iterations until equilibrium is reached for this increment.

Abaqus uses the full Newton Raphson method, i.e the model's stiffness matrix is updated in each iteration and the system of equations are solved for each iteration in this nonlinear analysis. This is very time consuming, since the tangential stiffness has to be formed and assembled in each iteration but the advantage is a very fast convergence. Abaqus also has an automatic increment control, so if the solution appears to diverge then it will restart the increment with a smaller increment length and if the solution converges easily then the increment length is increased for the next increment.

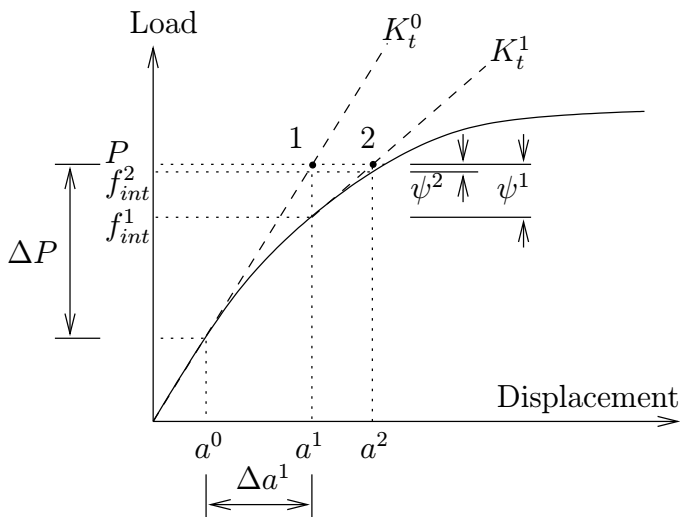


Figure 3.3: Graph illustrating the equilibrium iterations of an increment.

Iteration scheme for a displacement controlled analysis using the full Newton-Raphson method.

- Initiation of quantities  $\epsilon_0, \mathbf{K}_t, \mathbf{a}_0$
- For increment  $\text{inc}=1,2, \dots, N_{max}$ 
  - Set boundary condition to load the body
  - Set  $\boldsymbol{\psi}^i = \mathbf{0}$
  - Set  $\boldsymbol{\psi}_{norm} > tolerance$
  - Iterate while  $\boldsymbol{\psi}_{norm} > tolerance$ 
    - Calculate the tangential stiffness matrix,  $\mathbf{K}_t$
    - Calculate  $\Delta \mathbf{a}^i$  from  $\mathbf{K}_t \Delta \mathbf{a}^i = \boldsymbol{\psi}^i$
    - Set boundary condition to zero
    - Calculate  $\Delta \boldsymbol{\epsilon}^i = \mathbf{B} \Delta \mathbf{a}^i$
    - Calculate internal forces  $\mathbf{f}_{int}$
    - Calculate out-of-balance forces  $\boldsymbol{\psi}^{i+1} = -\mathbf{f}_{int}$
    - Calculate  $\boldsymbol{\psi}_{norm} = |\boldsymbol{\psi}^{i+1}|_{norm}$
  - End iteration
  - Accept quantities  $\boldsymbol{\epsilon}, \boldsymbol{\sigma}, \mathbf{a}, \mathbf{F}_{int}$
- End increment

### 3.6 Damped postbuckling

Abaqus may run into difficulties when local buckling of the corrugated board starts to occur. This problem and a method of solving this, is described in the Abaqus manual [8]. *"If the instability is localized, there will be a local transfer of strain energy from one part of the model to neighbouring parts and global solution methods do not work. This class of problems has to be solved either dynamically or with the aid of (artificial) damping; for example, by using dashpots. Abaqus provides an automatic mechanism for stabilizing unstable static problems through the automatic addition of volume proportional damping to the model".*

If the STABILIZE parameter is included in the input file, then viscous forces

$$\mathbf{F}_v = c\mathbf{M}\dot{\mathbf{a}} \quad (3.7)$$

are added to the global equilibrium equations.

$$\mathbf{P} - \mathbf{f}_{int} - \mathbf{F}_v = 0 \quad (3.8)$$

$\mathbf{M}$  is an artificial mass matrix,  $c$  is a damping coefficient and  $\dot{\mathbf{a}}$  is the vector of nodal velocities. While the buckling is stable, the viscous energy dissipated is very small, but when local instabilities occur and the local velocities increase then the strain energy is dissipated by the applied damping. The damping coefficient,  $c$ , is calculated so that the dissipated energy is a small fraction of the strain energy in the first increment. The value of this fraction, called the dissipation intensity, is by default  $2.0 \times 10^{-4}$ , but should be specified by the user so that the influence of the applied damping is as small as possible.

### 3.7 Failure criteria of the facings

One of the most commonly used criterion for material failure of paper loaded in-plane is the Tsai-Wu tensor polynomial criterion [9]. The relations between the stresses in the Cartesian coordinate system and the stresses in the spherical coordinate system are

$$\begin{aligned} \sigma_{11} &= \sigma^R \sin \phi \cos \theta \\ \sigma_{12} &= \sigma^R \sin \phi \sin \theta \\ \sigma_{22} &= \sigma^R \cos \phi \end{aligned} \quad 0 \leq \phi \leq \pi, 0 \leq \theta \leq 2\pi \quad (3.9)$$

where  $\sigma^R$  is the length of the stress vector  $\boldsymbol{\sigma}$ , see figure 3.4.

The Tsai-Wu failure criterion in a spherical coordinate system is then

$$\begin{aligned} (F_{11}n_{11}^2 + F_{22}n_{22}^2 + F_{66}n_{12}^2 + 2F_{12}n_{11}n_{22}) (\sigma_{tw}^R)^2 + \\ (F_1n_{11} + F_2n_{22}) \sigma_{tw}^R - 1 = 0, \quad \sigma_{tw}^R > 0 \end{aligned} \quad (3.10)$$

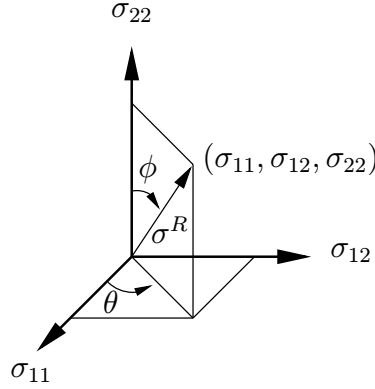


Figure 3.4: The stress vector in the Cartesian coordinate system.

where

$$n_{11} = \sin \phi \cos \theta \quad n_{12} = \sin \phi \sin \theta \quad n_{22} = \cos \phi \quad (3.11)$$

and

$$F_1 = \frac{1}{X_t} + \frac{1}{X_c}, F_2 = \frac{1}{Y_t} + \frac{1}{Y_c}, F_{11} = -\frac{1}{X_t X_c}, F_{22} = -\frac{1}{Y_t Y_c}, F_{66} = \frac{1}{T^2} \quad (3.12)$$

- $X_t$  = Tensile strength in MD
- $X_c$  = Compressive strength in MD
- $Y_t$  = Tensile strength in CD
- $Y_c$  = Compressive strength in CD
- $T$  = Shear strength

$\sigma_{tw}^R$  is the failure stress radius for material failure.

The tensile and compressive strength for both MD and CD must be determined by experimental tests. Because of the difficulties to determine the shear strength,  $T$ , and the equibiaxial strength,  $F_{12}$ , by experimental tests some approximations are used that have been proven to be reasonable for paper [10, 11].

$$F_{12} = f \sqrt{F_{11} F_{22}} \quad \text{where } f = -0.36 \quad (3.13)$$

$$T = \alpha \sqrt{X_c Y_c} \quad \text{where } \alpha = 0.78 \quad (3.14)$$

The critical stress for structural failure [12], i.e. when the facings becomes instable due to local buckling, can be calculated with

$$\sigma_{cr}^R = \frac{\sum_{i=1}^{33} g_i}{60a^2 h \lambda^2 (-c_2 n_{11} + 2a^2 \mu |n_{12}| - a^2 n_{22}) \sum_{i=1}^{27} h_i} \quad (3.15)$$

$$\sigma_{cr}^R > 0, \quad [\lambda, \mu] \in \mathbf{x}_{cr}$$

where  $h$  is the thickness of the facing,  $2\lambda$  is the buckling wavelength,  $\mu$  is the inclination of nodal lines and  $a$  is the wavelength of the corrugated core, see figure 3.5. The coefficients  $g_i$  and  $h_i$  are described in [13].  $\sigma_{cr}^R$  is the failure stress radius for structural failure and the numerical value of this parameter can be found by an unconstrained minimization procedure. A failure index can then be calculated as

$$\Phi(\sigma_{11}, \sigma_{12}, \sigma_{22}) = \frac{\|\boldsymbol{\sigma}\|}{\sigma_f^R} \quad (3.16)$$

where

$$\sigma_f^R = \min \{ \sigma_{tw}^R, \sigma_{cr}^R \} \quad (3.17)$$

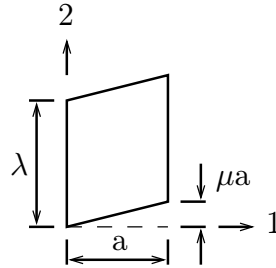


Figure 3.5: Buckle subjected to transverse shear.



# Chapter 4

## Finite element analysis

In this chapter are the finite element analyses of the detailed model and the simplified model described as well as the post-processor developed in Matlab for visualization of the local buckling.

### 4.1 Detailed model

This section describes how the corrugated paper board is modelled by the finite element method with veritable geometry.

#### 4.1.1 Geometry modelling

The board dimensions are given by the available test equipment. The test rig is designed to fit in a quadratic panel of 400 mm width. The fluting is shaped approximately as a sine wave and has a wavelength of 7.77 mm. The distance between the two liners are 3.68 mm as shown in figure 4.1.

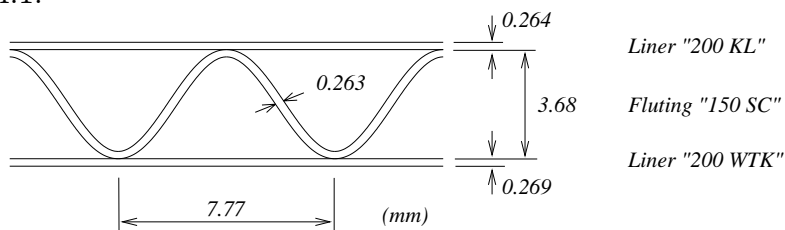


Figure 4.1: Dimensions of the corrugated paper board.

In order to translate the geometry to a FE model some basic assumptions has to be made. Of course, the fluting cannot be modelled with a perfect sine shape, figure 4.2 and in order to avoid constraint equations, the contact nodes between fluting and liner are modelled without offset, figure 4.3. Because the fluting and liner are connected to the same node, the bending stiffness of the fluting to liner connections will be overestimated. The coordinates of the nodes for the fluting are adjusted so that the length of the fluting elements will be almost the same.

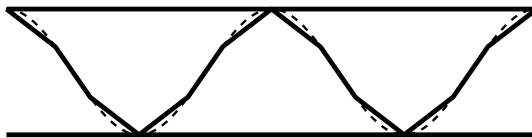


Figure 4.2: Shape of the fluting.

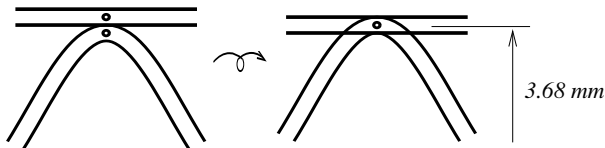


Figure 4.3: Model with and without offset.

### 4.1.2 Material modelling

The material behaviour is orthotropic, as seen in section 3.2, and approximated as linear-elastic. This approximation is made because no nonlinear material model suitable for paper was available, and to reduce the computation time. The FEA is taking large deformations in account and if the material behaviour also would be nonlinear, the number of iterations would have increased significantly. This would, having approximately 400000 degrees of freedom in the model, give an unendurably long computation time.

The material parameters,  $E_x$  and  $E_y$  are from experimental measurements.  $E_z$  and  $G_{xy}$  are calculated according to (3.3) and (3.4), respectively and the Poisson's ratios are set according to [14]. These parameters, which are the same for all analyses, are presented in table 4.1. Since

the shear moduli,  $G_{xz}$  and  $G_{yz}$ , are difficult to estimate, three analyses were performed with different values of these parameters. The different values used in the analyses were, values suggested by Nordstrand [14], (No. 3), values calculated with Baum's approximations (3.4), (No. 1), and values adjusted to fit the load versus out-of-plane displacement curves from the tests, (No. 2). The values of  $G_{xz}$  and  $G_{yz}$  for the three analyses are presented in table 4.2. The tensile and compressive strength parameters in table 4.3 are determined from experimental tests and are used for the failure criteria.

Table 4.1: Material parameters for the three layers.

	Liner 200 WTK	Fluting 150 SC	Liner 200 KL
$E_x$ (GPa)	7.60	5.40	6.66
$E_y$ (GPa)	4.02	2.28	3.31
$E_z$ (GPa)	0.038	0.027	0.033
$\nu_{xy}$	0.34	0.34	0.34
$\nu_{xz}$	0.01	0.01	0.01
$\nu_{yz}$	0.01	0.01	0.01
$G_{xy}$ (GPa)	2.14	1.36	1.82
Thickness (mm)	0.269	0.263	0.264

Table 4.2: Values of  $G_{xz}$  and  $G_{yz}$  for the three layers.

		200 WTK	150 SC	200 KL
No. 1	$G_{xz}$ (GPa)	0.138	0.098	0.121
	$G_{yz}$ (GPa)	0.115	0.065	0.095
No. 2	$G_{xz}$ (GPa)	0.020	0.020	0.020
	$G_{yz}$ (GPa)	0.070	0.065	0.070
No. 3	$G_{xz}$ (GPa)	0.007	0.007	0.007
	$G_{yz}$ (GPa)	0.070	0.070	0.070

Table 4.3: Tensile and compressive strength parameters of the layers.

	200 WTK	150 SC	200 KL
$F_x^t$ (MN)	90.0	50.0	68.6
$F_x^c$ (MN)	27.7	21.8	25.1
$F_y^t$ (MN)	49.2	20.6	40.1
$F_y^c$ (MN)	19.7	13.3	17.9

### 4.1.3 Finite element mesh

The first step in a FEA is to decide what kind of elements to use and how dense the FE mesh has to be in order to obtain valid results.

Due to the high degree of orthotropy, the transverse shear deformation is important and a thick shell element must be chosen. To save computation time reduced integration is chosen. This also usually provides more accurate results, since otherwise the stiffness of the finite elements would be overestimated. Considering this, the Abaqus elements S4R and S8R are possible choices. S4R is a four-node quadrilateral thick shell element, see figure 4.4, with linear shape functions and S8R is an eight-node element with quadratic shape functions. Two identical analyses, eigenvalue buckling analyses of a small part of the board, with the two types of elements showed that there is no significant difference in the results between them, when the same number of elements are used. The model just becomes larger for S8R. Therefore, S4R is chosen. The global coordinate system coincides with the local coordinate system for the liner elements but not for the fluting elements, because of the wavy shape of the fluting. The output stresses and strains are given in local coordinates, i.e. the coordinates of the deformed shell.

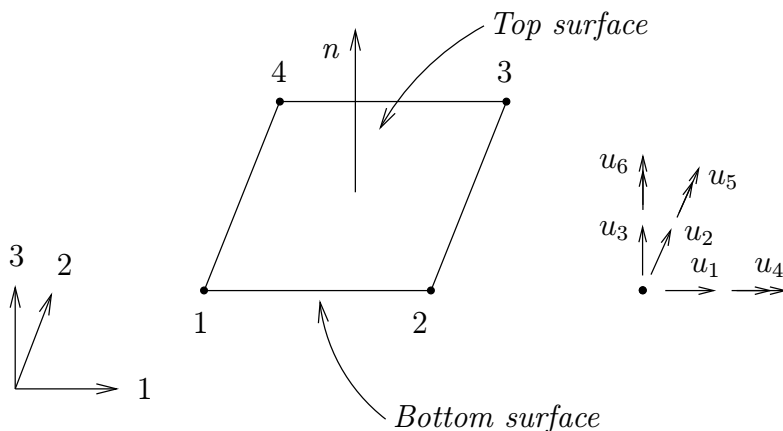


Figure 4.4: Element definition for four-node quadrilateral shell element and the definition of the degrees of freedom.

To decide the size of the elements a convergence study was performed. In this case an eigenvalue bifurcation prediction was performed, see chapter 3.4, for a small plate, see figure 4.5. The width of the simply supported

plate,  $a$ , is the same as the length between the corrugations, i.e. 7.77 mm. The appropriate wave length  $\lambda$  is, for the case when only pure bending is considered, calculated with (4.1), see [15], and for the case when transverse shear also is considered calculated by minimization of (3.15) [16]. For liner 200 WTK the appropriate lengths are 6.63 mm and 7.18 mm respectively.

$$\frac{\lambda}{a} = \sqrt[4]{\frac{E_y}{E_x}} \quad (4.1)$$

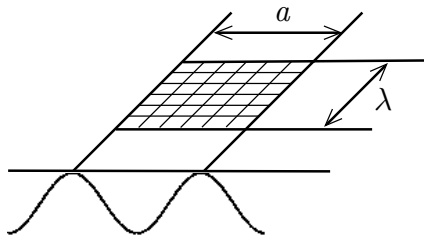


Figure 4.5: Part of the liner used in the convergence study.

As seen in figure 4.7, five elements would be sufficient to capture local buckling. However, since an evenly distribution of elements is necessary to obtain a correct junction between the liner and fluting elements, six elements were chosen. This yields a model with 73008 elements and 398926 degrees of freedom.

Another thing to keep in mind is the output from Abaqus. Since the Simpson's integration rule is used, the default output will be the section points that are located exact on the bottom surface and top surface of the shell element.

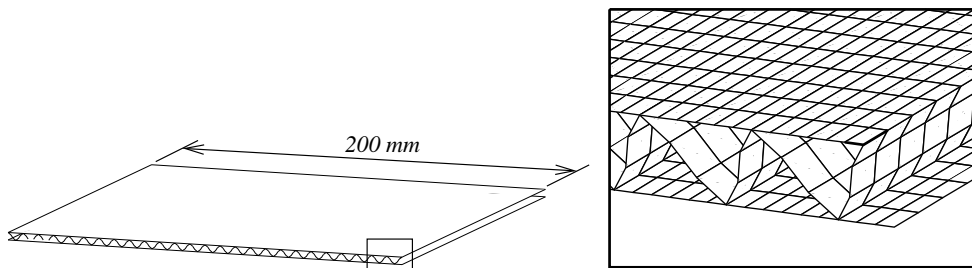


Figure 4.6: Finite element mesh.

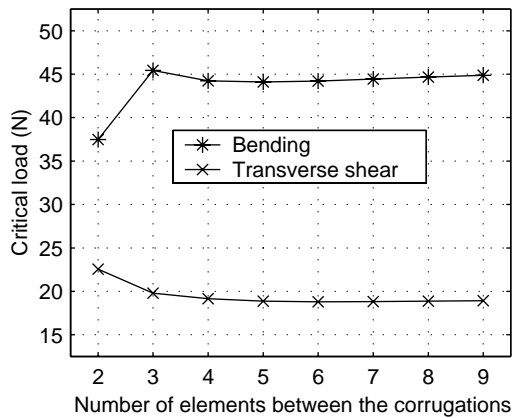


Figure 4.7: Convergence study of mesh.

#### 4.1.4 Boundary conditions

The aim was to model the boundary conditions as close as possible to the testing mounting, see section 5.1.1. The panel is considered to be simply supported. To obtain the same behaviour in the FEA, some constraint equations had to be established for the boundary edge subjected to load. At the symmetry boundaries one translation and two rotations are prescribed, see figure 4.8. For example at the symmetry boundary where  $x$  is constant, the degrees of freedom, see figure 4.4,  $u_1$ ,  $u_5$  and  $u_6$  are set to zero. At the other symmetry boundary, where  $y$  is constant, the degrees of freedom  $u_2$ ,  $u_4$  and  $u_6$  are set to zero. At the boundary where  $x$  is 0, the degrees of freedom  $u_3$  and  $u_4$  are set to zero.

Now only the loaded boundary remains. If the load is applied as a boundary condition on all the nodes on the edge, the rotation  $u_4$  is prevented. This leads to an almost fixed support for these nodes. To avoid this, the load is instead applied on a master node that is not involved in the structure. This master node must then be connected to the boundary nodes with constraint equations to control the motion of the boundary nodes. Note that only degree of freedom  $u_2$  is active for the master node. This since the node is not connected to any element and the only way it participates in the calculations is by the prescribed translation in the  $y$ -direction. The purpose of the constraint equations is to allow rotation about the  $x$ -axis and to keep a plane edge during the compression, see figure 4.9.

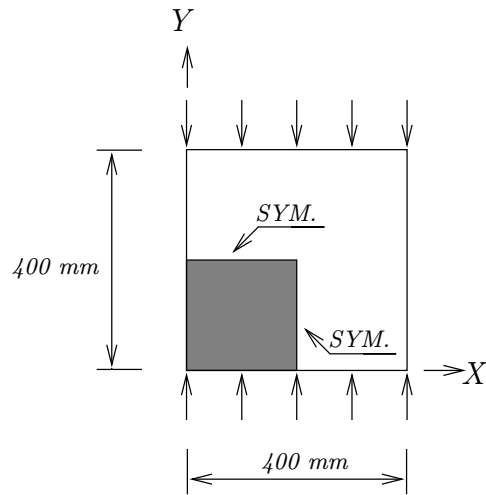


Figure 4.8: The studied quarter of the board with symmetry lines.

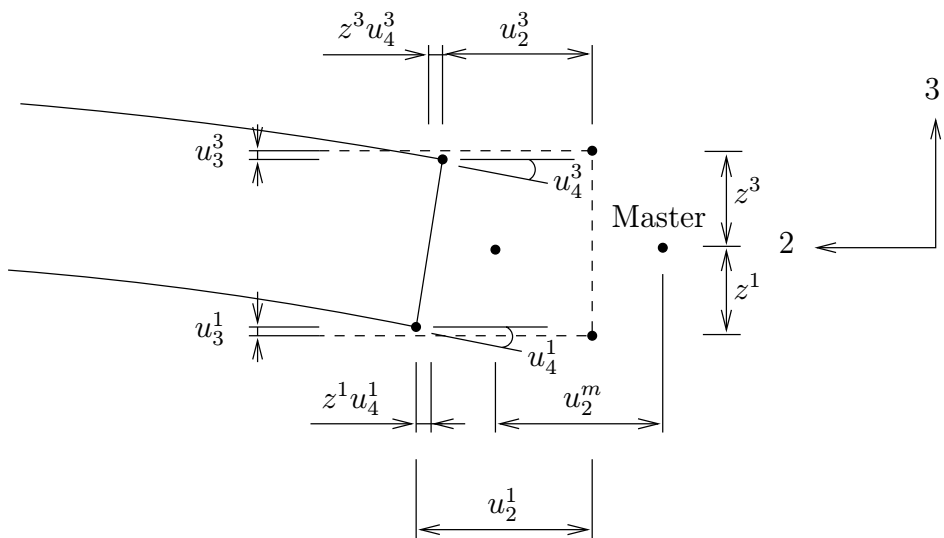


Figure 4.9: The loaded boundary that is controlled by constraint equations.

The translation in the  $y$ -direction is for all nodes described by

$$u_2^n + z^n u_4^n - u_2^m = 0 \quad (4.2)$$

where  $n$  denotes layer and  $m$  denotes the master node. The rotation about the  $x$ -axis

$$\begin{cases} u_4^1 - u_4^2 = 0 \\ u_4^2 - u_4^3 = 0 \end{cases} \quad \text{or} \quad u_4^1 - u_4^3 = 0 \quad (4.3)$$

The translation in the  $z$ -direction

$$u_3^1 + u_3^3 = 0 \quad (4.4)$$

## 4.2 Buckling

The linear buckling analysis, described in section 3.4, is performed to obtain the most likely buckling shape and an estimation of the critical buckling load. This buckling shape is used as an imperfection in the nonlinear analysis. The results also provides an opportunity, in the post processor, to visually control that the boundary conditions are correct, by the shape of the deformed panel. A reference load is applied and the critical buckling load is calculated by multiplying the eigenvalue from the analysis by the reference load.

## 4.3 Postbuckling

The geometrically nonlinear behaviour requires an incremental technique to follow the load path, as described in section 3.5. To reflect the experimental tests, the FEA is displacement controlled. An imperfection might be necessary for several reasons. One is that the panels used in the tests possessed imperfections. Another reason is that a numerical solution to the buckled shape might not be possible if the panel is geometrically perfect. A typical 400x400 mm panel showed an imperfection of 0.8 mm in the centre. Also a damped postbuckling analysis, described in section 3.6, might be necessary to overcome the numerical problems when a bifurcation point is reached.

In the input file to Abaqus some loading parameters have to be defined. These are, the total deformation value, the maximum number of increments in a step, the initial displacement increment, the time period of the step, the minimum displacement of an increment and the maximum displacement increment. A parameter that makes Abaqus take account for geometric nonlinearity in the calculations must be included and if the STABILIZE-option is chosen, then the value of the dissipation intensity also should be defined.

The results that are wanted from the FEA are:

- A load-displacement path, to follow the applied load and out-of-plane displacement.
- Surface plots of the Tsai-Wu failure criterion.
- Surface plots of the failure index given by (3.16).
- Surface plots of the deformations, to follow the development of the deformations and the local buckling.
- Surface plots of strains and stresses.

## 4.4 Simplified model

In order to verify if a simplified composite model provides satisfying results in terms of load-deformation path and collapse load, a composite model with a solid core was created, see figure 4.10. The material pa-

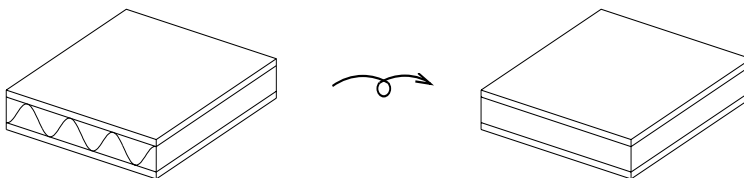


Figure 4.10: Transformation to a composite model.

rameters of the facings are the same as in section 4.1.2, which imply that three analyses must be performed also for the simplified model. Since the fluting has been replaced with a core, the equivalent properties for this

layer needs to be calculated. According to Nordstrand [14] the effective core moduli can be approximated as

$$\begin{aligned} E_x^c &\approx 0 \\ E_y^c &\approx \alpha \left( \frac{t_f}{t_c} \right) E_{CD}^c \end{aligned} \quad (4.5)$$

where  $\alpha$  is the take-up factor,  $t_f$  is the thickness of the flute material and  $t_c$  is the core height.  $\alpha$  is the ratio between the arclength and the wavelength of the corrugations, which is 1.416 for a sine shaped fluting. If  $E_x^c$  is set to zero there will be numerical difficulties in the FEA and the analysis will be terminated. Therefore,  $E_x^c$  is set to a low value that does not affect the analysis. The lowest value possible for  $E_x^c$  was 5 MPa and this was used in the calculations.  $G_{xy}^c$  should also be a low value [14] and is therefore set to 0.1% of  $E_y^c$ . The values of  $G_{xz}^c$ ,  $G_{yz}^c$ ,  $E_z^c$ ,  $\nu_{xy}^c$ ,  $\nu_{xz}^c$  and  $\nu_{yz}^c$  are set according to Nordstrand [14]. The material parameters that are similar in the three analyses are seen in table 4.4 and the ones that differ are presented in table 4.5.

Table 4.4: Material parameters for the layers of the composite.

	Liner 200 WTK	Core	Liner 200 KL
$E_x$ (MPa)	7600	5.0	6660
$E_y$ (MPa)	4020	231	3310
$E_z$ (MPa)	38	3000	33
$\nu_{xy}$	0.34	0.05	0.34
$\nu_{xz}$	0.01	0.01	0.01
$\nu_{yz}$	0.01	0.01	0.01
$G_{xy}$ (MPa)	2140	0.231	1820
Thickness (mm)	0.269	3.677	0.264

In Abaqus there is a command that handles layered composite shell elements so that the user only has to create one layer of nodes and then specify the properties of the three materials. The 200x200 mm panel was divided into 2500 composite elements which yields 15606 degrees of freedom. Because there is only one layer of nodes no equations, as in section 4.1.4, are needed to prescribe the correct boundary conditions at the loaded edge. Besides this, the analysis is performed in the same manner as for the model with the structural core.

Table 4.5: The different values of  $G_{xz}$  and  $G_{yz}$  for the layers of the composite.

		200 WTK	Core	200 KL
No. 1	$G_{xz}$ (MPa)	138	3.5	121
	$G_{yz}$ (MPa)	115	35	95
No. 2	$G_{xz}$ (MPa)	20	3.5	20
	$G_{yz}$ (MPa)	70	35	70
No. 3	$G_{xz}$ (MPa)	7	3.5	7
	$G_{yz}$ (MPa)	70	35	70

## 4.5 Matlab post-processor

When the calculations are performed in Abaqus the numerical results can be post-processed by Abaqus/Viewer. Since the calculation is performed in numerous increments, which each is saved in the output data files, this becomes a very time consuming process. One of the main purposes in this master thesis was to study local buckling. Therefore, it was of great importance to visualize the occurrence of this phenomena. In Abaqus/Viewer this is not possible, since the, in comparison to the global out-of-plane displacement, small buckles disappear in the global deformation.

To avoid the above stated problems, a new post-processor was developed. The interesting information that should be presented by the post-processor was load-deformation path, displacements, stresses, strains and the failure index for each increment.

In order to obtain the local buckling pattern of the board, the global deformation mode has to be filtrated, see figure 4.11. This was done by subtracting the global out-of-plane displacement, from the total out-of-plane displacement for each node. The difference in out-of-plane displacement between the two end nodes of a corrugation,  $u_3^i$  and  $u_3^{i+6}$ , is calculated. These displacements are equal to both the global and the total out-of-plane displacements. Then the linear interpolated value of the global out-of-plane displacement for the nodes between these are calculated, e.g.  $u_{3,g}^{i+2}$ , and subtracted from the total out-of-plane displacement,  $u_3^{i+2}$ . The remaining deformation is the displacement caused by local buckling,  $u_{3,l}^{i+2}$ .

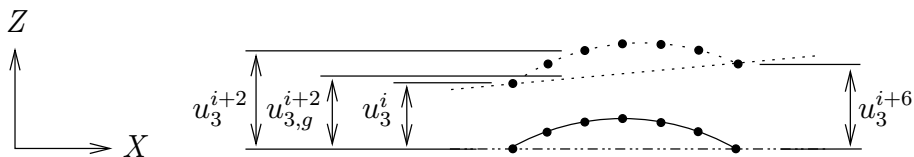


Figure 4.11: Calculation of local deformation.

$$\begin{aligned}
 u_{3,g}^{i+j} &= [(u_3^{i+6} - u_3^i) / (x^{i+6} - x^i)] (x^{i+j} - x^i) + u_3^i \\
 u_{3,l}^{i+j} &= u_3^{i+j} - u_{3,g}^{i+j} \quad \text{where} \quad 0 \leq j \leq 6
 \end{aligned}
 \tag{4.6}$$

To get the wanted results from the calculations, the resultsfile, "job-name".fil was used. The output data from each increment was extracted from the resultsfile with Fortran routines and then it was exported to .mat files for evaluating in Matlab. In Fortran was also the calculations, that was needed to obtain the local deformations, performed. In order to easily change which type of result to present, a graphical user interface was developed in Matlab, see figure 4.12. By using this, it is easy to choose which increment and layer to study. With the use of the menus and buttons the different kind of results can be changed.

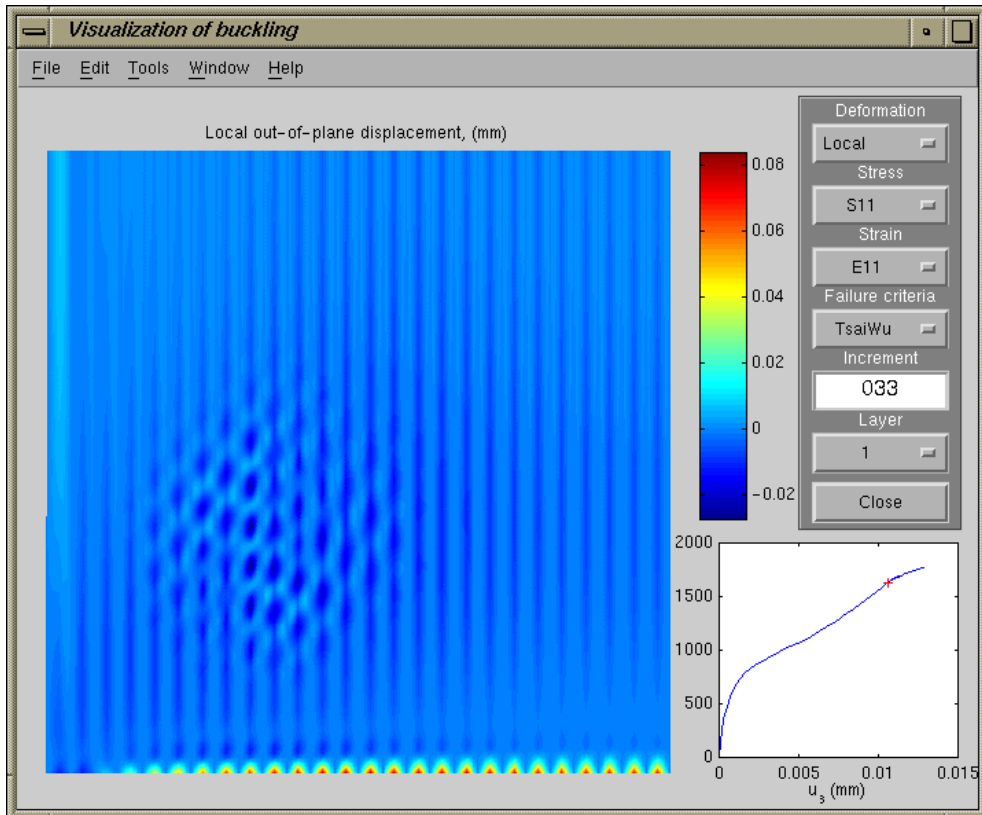


Figure 4.12: Screen-dump of the post-processor developed in Matlab.

## 4.6 Results

### 4.6.1 Detailed model

The output from the linear buckling analysis, as mentioned in section 4.2, is the pertinent buckling shape and provides an estimate of the critical buckling load. The most likely shape of the panel is the first mode, see figure 4.13, and the critical loads for the three analysis are given in table 4.6.

Table 4.6: Critical buckling load for detailed model.

Material	$N_{cr}$ (N)
No. 1	955
No. 2	935
No. 3	902

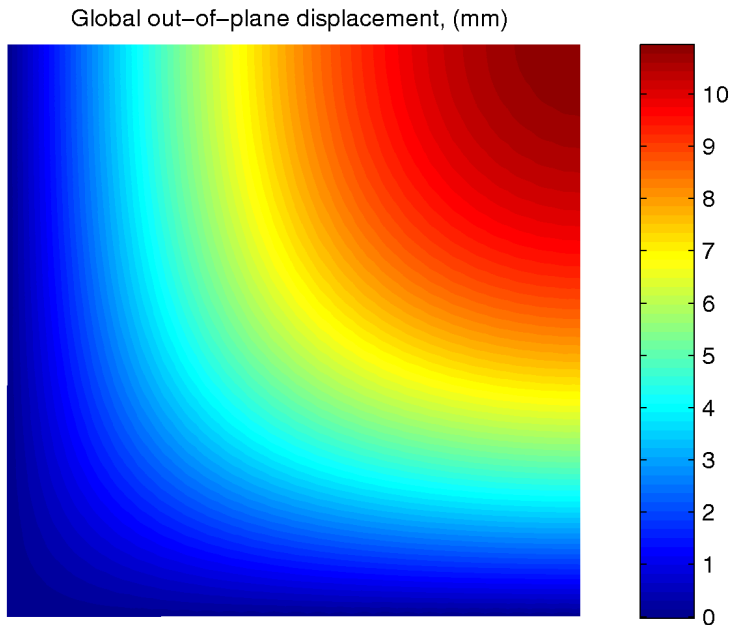


Figure 4.13: Global out-of-plane displacement for the detailed model No. 2. Load = 1580 N.

Because of the convergence problems in the FEA at singular points, the artificial damping described in section 3.6 had to be introduced. The influence of the applied damping was large when using the default value ( $2 \times 10^{-4}$ ) of the dissipation intensity. Therefore, this coefficient was decreased and set to  $2 \times 10^{-5}$  to minimize the influence, see figure 4.14, but still to overcome the singular points in all analysis. Although, it is possible to decrease the dissipation intensity even more for some material configurations.

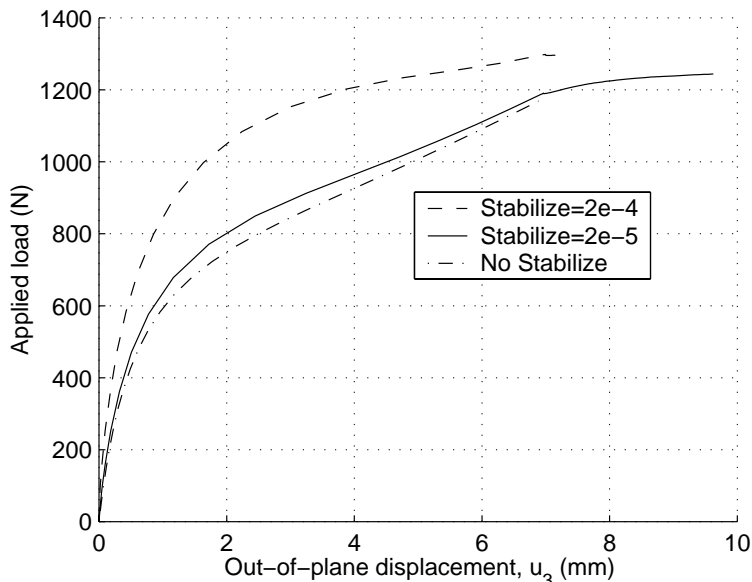


Figure 4.14: The influence of the applied damping for material No. 3.

The load-displacement response for the three different materials of the detailed model can be seen in figure 4.15. The shear moduli  $G_{xz}$  and  $G_{yz}$  are of great importance and have to be carefully determined. It is also seen that the critical load for structural failure is less than the critical load for material failure for weak materials. This implies that structural failure must be considered. The stiffness of the board increases after the first bifurcation point. This is due to the linear-elastic material model and the geometrical stiffness which increases with deformation.

An important issue to remember, is to check the boundary conditions so that the shape according to a simply supported plate is achieved, see figure 4.16.

There are warning messages for negative eigenvalues in the Abaqus .msg-

file, i.e. singular points where the eigenvalue changes from positive to negative. A singular point can either be a bifurcation point where the load-displacement curve can develop several paths or a point where the load has reached a local maximum [18]. This occurs, for the No. 2 and the No. 3 material, in the increments following after the increment where the structural failure index for local buckling exceeds 1.0, as seen in table 4.7. It can clearly be seen in figure 4.17 and 4.18 that the local buckling develops close after the first singular point.

The failure indices are presented, in figure 4.19, when the structural failure index exceeds 1.0 and in figure 4.20, when the material failure index exceeds 1.0. Note that, in figure 4.20, the local deformations have developed normal stresses that are not homogeneous in the thickness direction of the liner. Thus, the structural index should be treated with care.

Table 4.7: First negative eigenvalue in the FEA compared to structural and material failure.

Material	Negative eigenvalues		Struc. fail.		Mat. fail.	
	Inc.	Load (N)	Inc.	Load (N)	Inc.	Load (N)
No. 1	46	2254	36	1928	34	1858
No. 2	28	1615	27	1580	34	1630
No. 3	18	1187	16	1060	80	1232

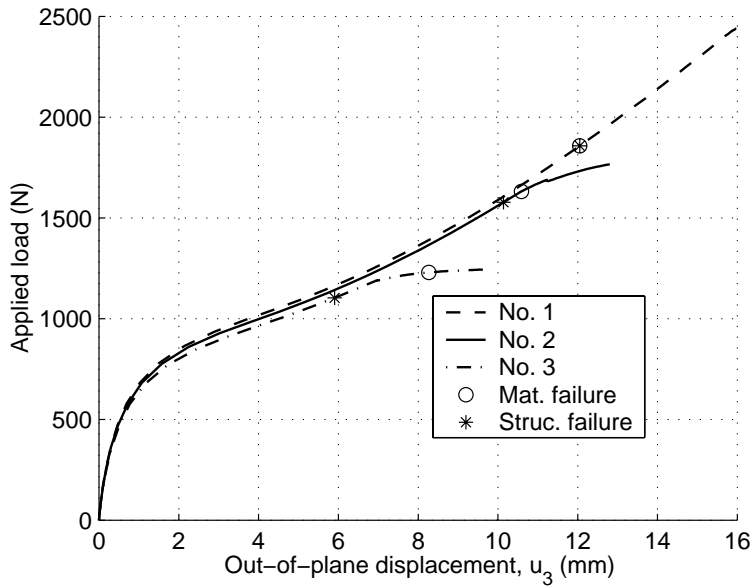


Figure 4.15: Load vs. out-of-plane displacement at point  $x = y = 200$  mm, for the three different materials.

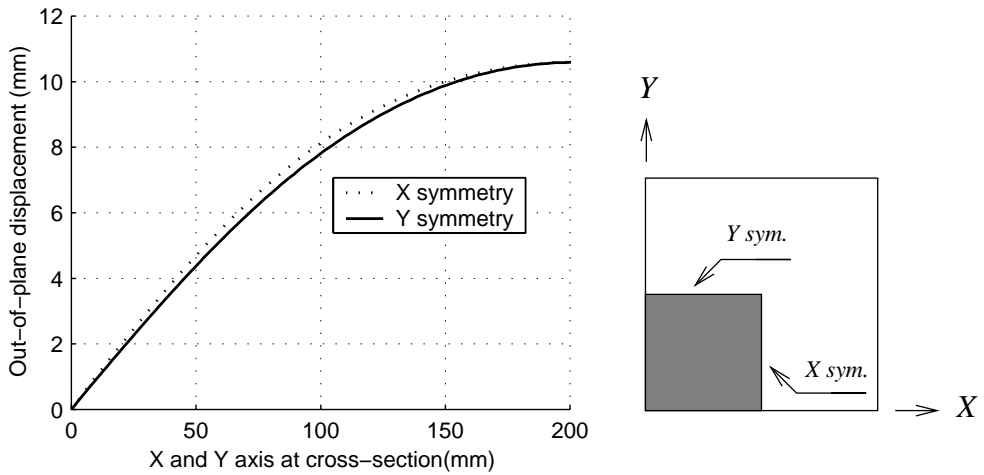


Figure 4.16: Shape at symmetry sections for detailed model.

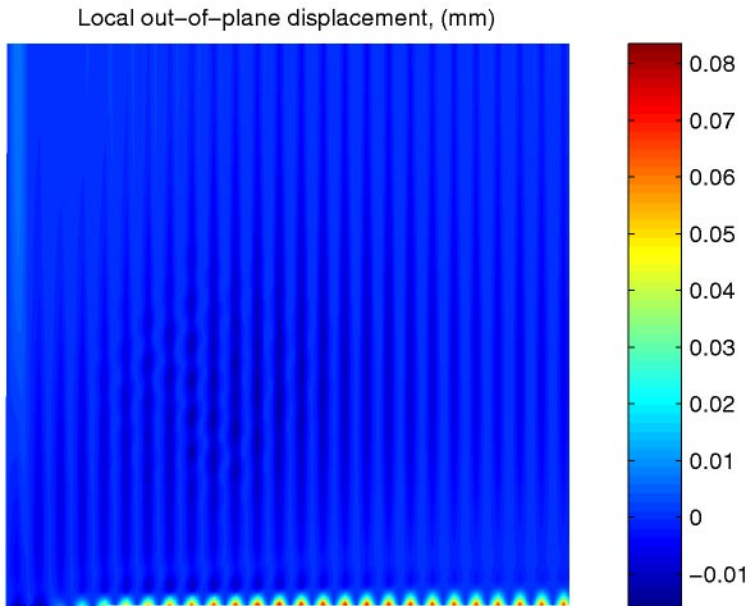


Figure 4.17: Local out-of-plane displacement for the detailed model No. 2 at increment 31. Load = 1627 N. Liner 200 WTK.

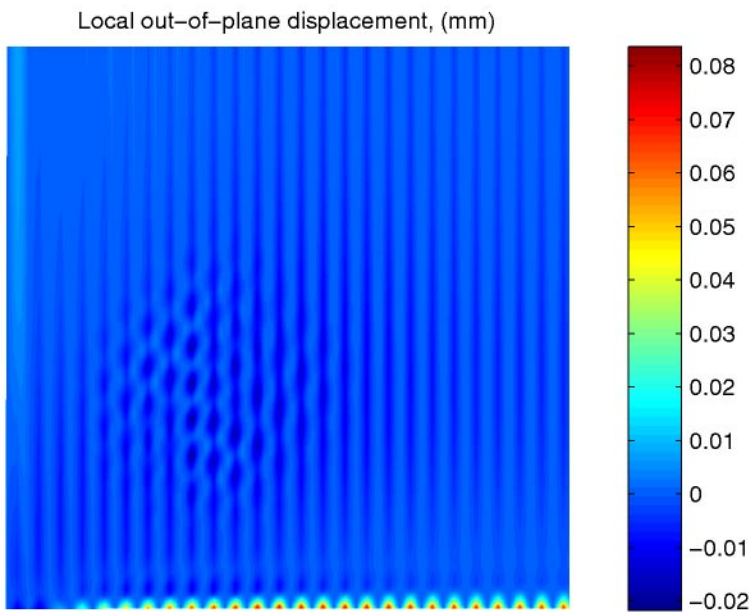


Figure 4.18: Local out-of-plane displacement for the detailed model No. 2 at increment 32. Load = 1628 N. Liner 200 WTK.

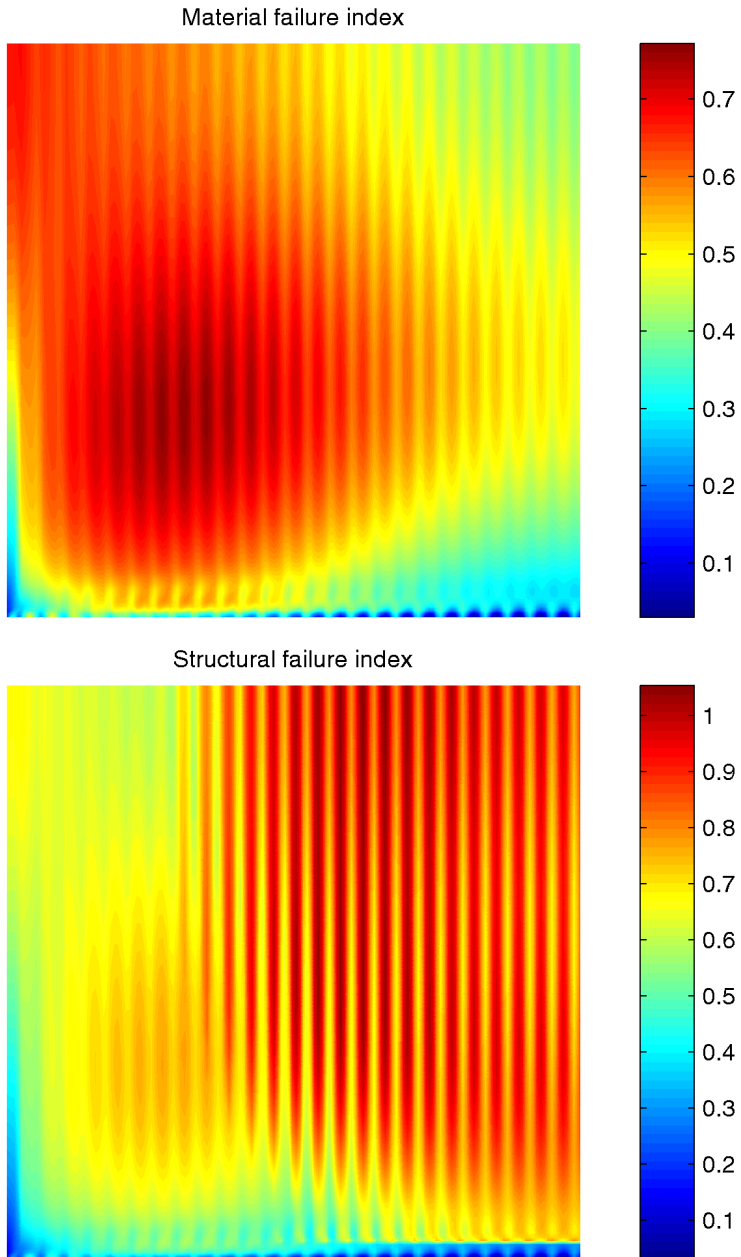


Figure 4.19: Material and structural failure criterion for the detailed model No. 2. Load = 1580 N. Liner 200 WTK.

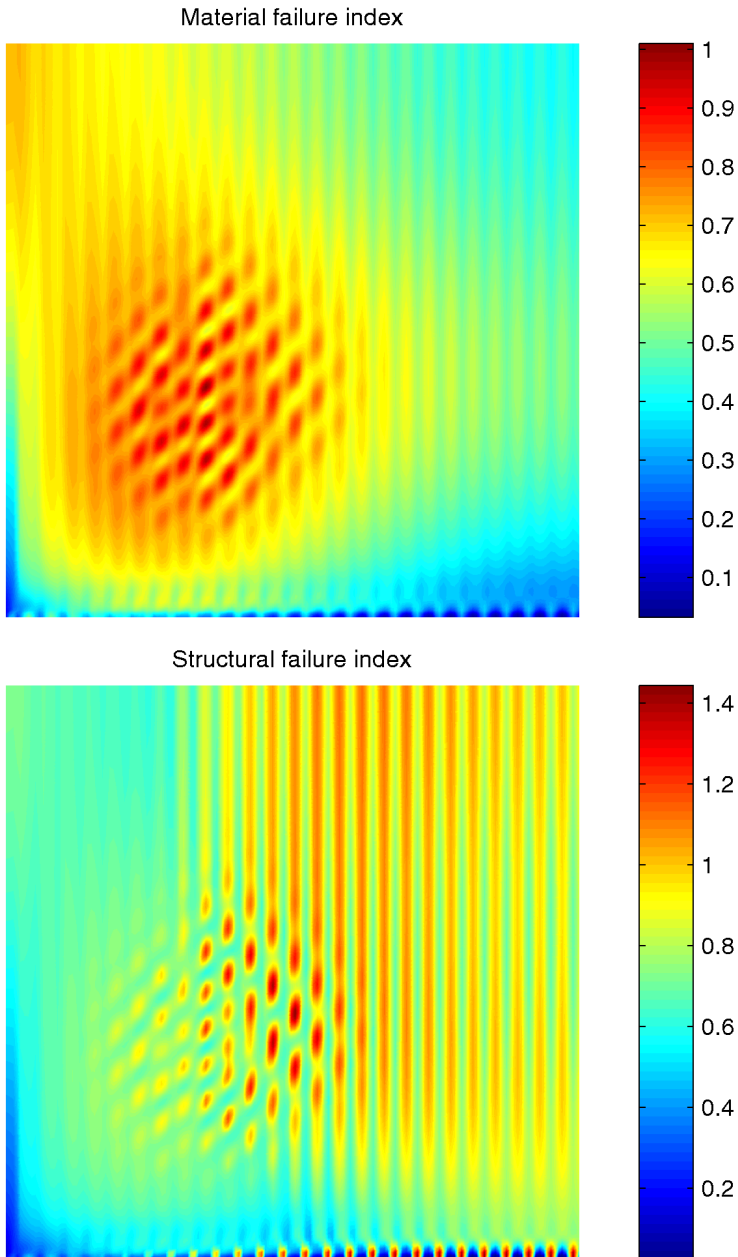


Figure 4.20: Material and structural failure criterion for the detailed model No. 2. Load = 1630 N. Liner 200 WTK.

### 4.6.2 Simplified model

The global deformation pattern of the panel is presented in figure 4.22, and the shape of the symmetry sections, in figure 4.21.

The shear moduli  $G_{xz}$  and  $G_{yz}$  are of less importance in this type of analysis because the liners are attached to the solid core and cannot buckle locally. This makes the differences between the three analyses very small as seen for the critical buckling loads from the linear buckling analysis in table 4.8, and the load-displacement paths in figure 4.23. The material failure index is also the same for the three analysis, while they differ substantially for structural failure. This is because the stresses do not depend (or very little) on the out-of-plane shear moduli,  $G_{xz}$  and  $G_{yz}$ , and the Tsai-Wu failure criterion does not consider the out-of-plane shear moduli as the structural failure criterion do.

The failure indices are presented in figure 4.24 and 4.25, when the combined and the material failure index exceeds 1.0, respectively.

Table 4.8: Critical buckling load for simplified model.

Material	$N_{cr}$ (N)
No. 1	1006
No. 2	1004
No. 3	1003

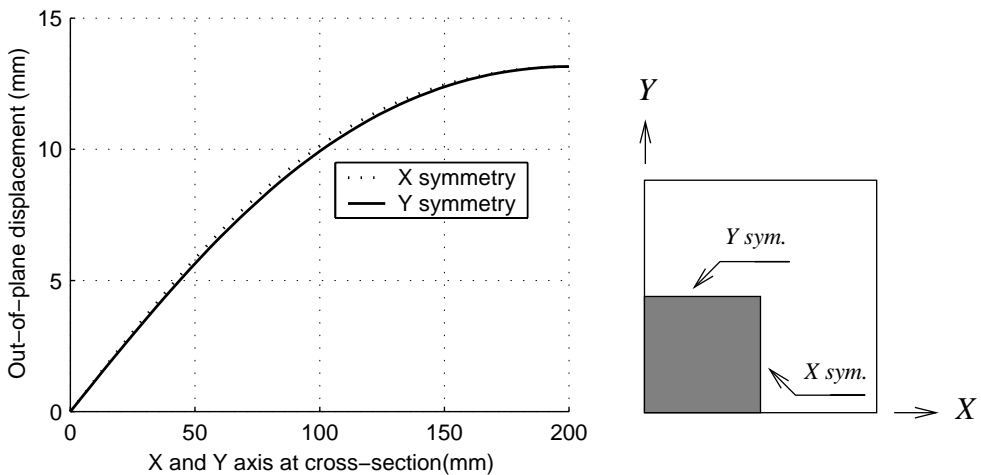


Figure 4.21: Shape at symmetry sections for simplified model.

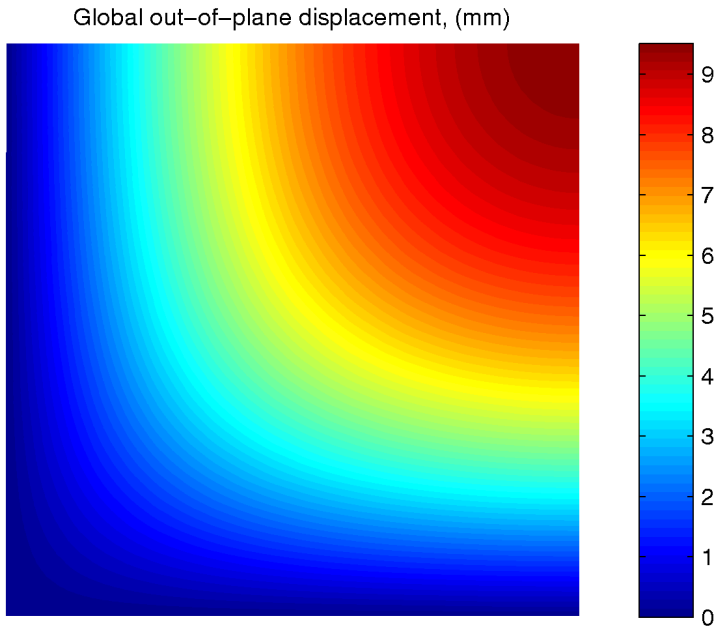


Figure 4.22: Global out-of-plane displacement for the simplified model No. 2. Load = 1582 N.

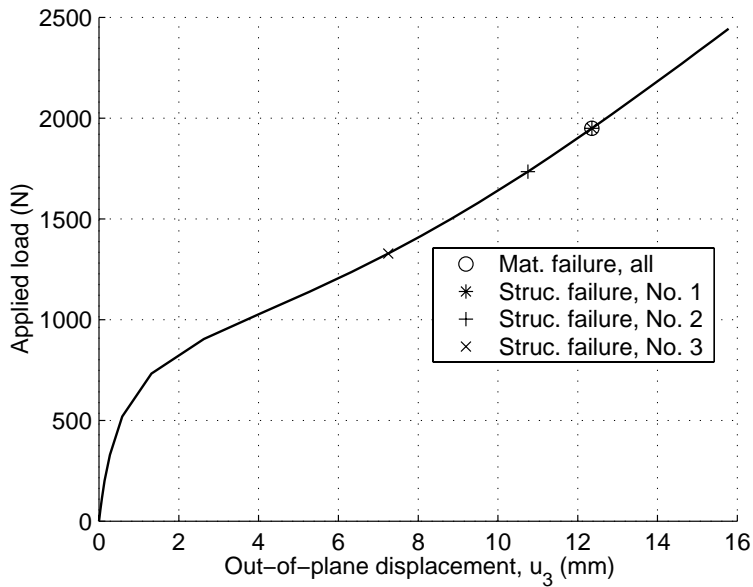


Figure 4.23: Load vs. out-of-plane displacement for the three different materials.

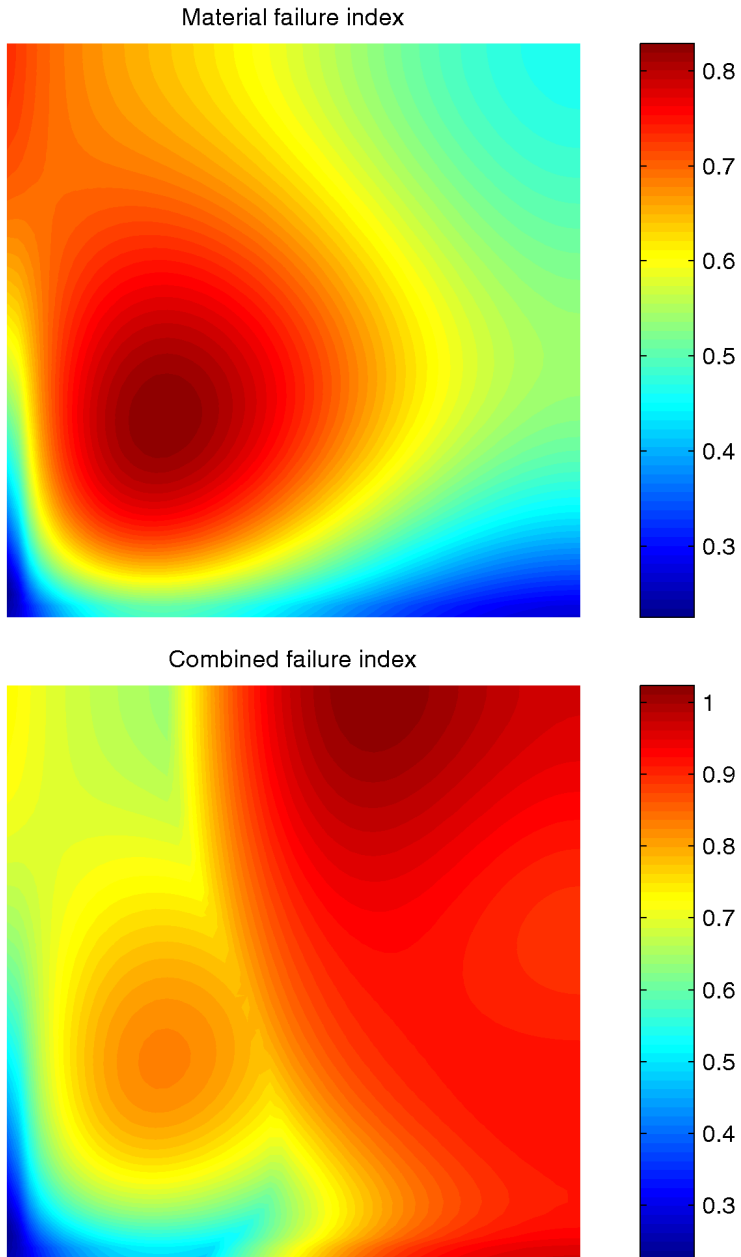


Figure 4.24: Material and combined failure criterion for the simplified model No. 2. Load = 1730 N. Liner 200 WTK.

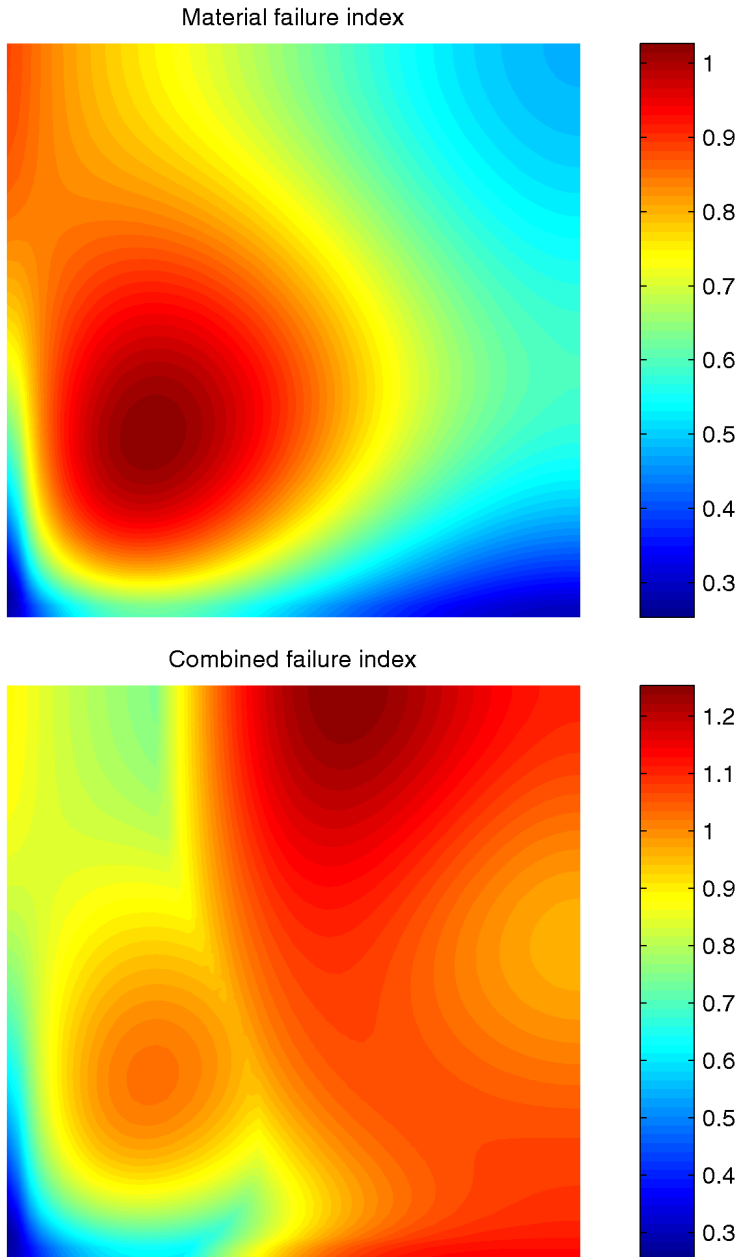


Figure 4.25: Material and combined failure criterion for the simplified model No. 2. Load = 1950 N. Liner 200 WTK.

# Chapter 5

## Experimental study

In order to verify the theoretical load-deformation response, obtained by finite element analysis, experimental compression tests on a corrugated board panel were performed at SCA Packaging Research in Sundsvall.

### 5.1 Equipment and set-up

The panel was loaded in compression in a displacement controlled MTS frame, see figure 5.1, that can register load and in-plane boundary displacement. To obtain in-plane and out-of-plane deformations of the corrugated board panel, stereoscopic Digital Speckle Photography (DSP) was used.

#### 5.1.1 MTS test frame

The MTS test frame has one movable crosshead between two fixed crossheads. Depending on the test, the specimen can be mounted either between the lower and the movable crosshead or the upper and the movable crosshead. In this test the axial load monitoring cell was mounted on the upper fixed crosshead and had a capacity of 2 kN, with a tolerance of 0.02%. Thus, the movable crosshead is moved upwards to compress the panel.

The panel is mounted, as seen in figure 5.2a, to be simply supported. If the horizontal supports would have been designed in the same way as the

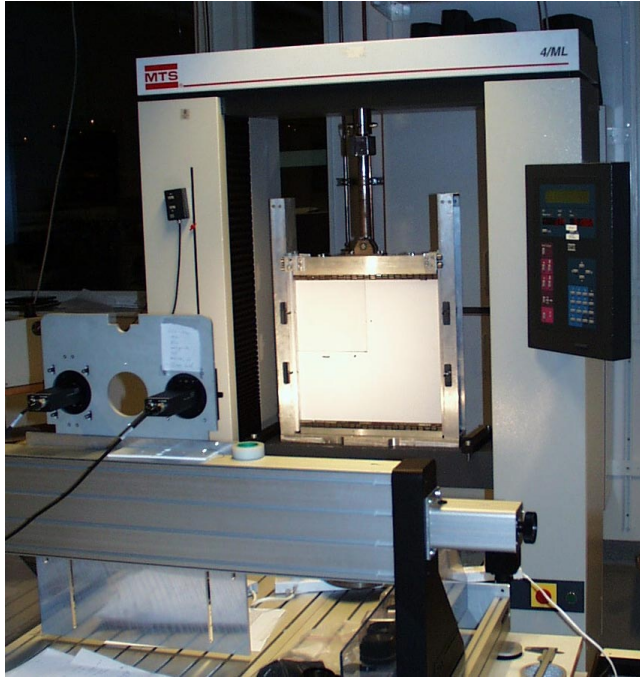


Figure 5.1: Photo of the MTS test frame and the two CCD-cameras.

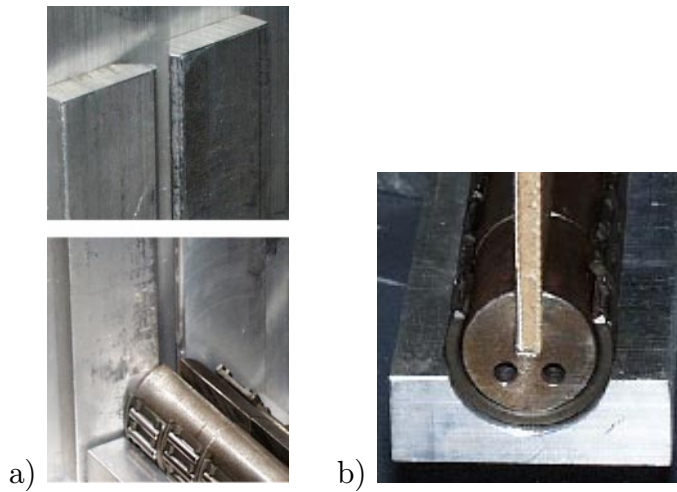


Figure 5.2: a) Photo of vertical and horizontal support. b) The panel mounted in the horizontal support.

vertical, the free rotation would have been restrained when compressed. Thus, the horizontal supports had to be designed differently, in this case as seen in figure 5.2b. This design makes, of course, the edge stiffer but it does not affect the results. Note that the panel has to be a few millimetres wider than the distance between the vertical supports to prevent it from falling off.

### 5.1.2 Digital Speckle Photography

The general procedure of speckle photography is to expose a photographic plate to one speckle field before and one after the object has been deformed. This negative, also referred to as a specklegram, can then be seen as two slightly displaced images. When a narrow laser beam is pointed on the specklegram a diffraction halo will appear, see figure 5.3. From this the in-plane displacements can be calculated. This procedure is very time consuming because each point has to be evaluated individually.

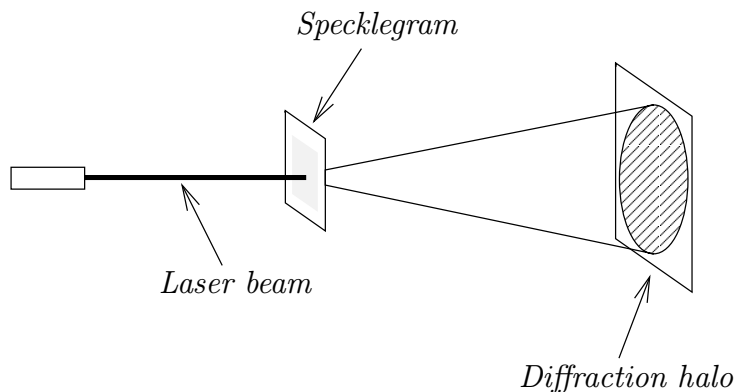


Figure 5.3: The general procedure of speckle photography.

To get a more time efficient line of work, Digital Speckle Photography, DSP, where the photographic plate is replaced with a CCD-camera and the analysis is made by a computer, was developed by Sjö Dahl [19]. It uses a digital image correlation technique to obtain the deformations with great accuracy. The DSP can be combined with a stereo imaging system to obtain three dimensional deformations [20], see figure 5.4. For a stereo-DSP system the standard deviation for the out-of-plane deformation component are less than 6% of the pixel size of the CCD-camera [21]. The standard deviation of the in-plane deformations are about 1% of the

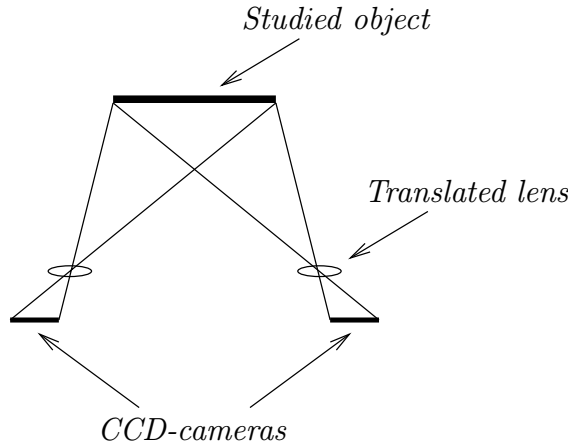


Figure 5.4: Basic configuration for stereoscopic vision using the translated lens method.

pixel size. With a 512x512 resolution of the CCD-camera and an object size of 200x200 mm the typical error for the out-of-plane and in-plane deformation is approximately  $23 \mu\text{m}$  and  $4 \mu\text{m}$  respectively. Compared to an out-of-plane deformation of a few millimetres this error is negligible.

## 5.2 Test procedure

Before the testing procedure is started a speckle pattern, i.e. a random pattern of small dots, is printed on the panels, see figure 5.5. The speckle pattern is printed on a quarter of the panel (symmetry) to increase the resolution and on a smaller part to study local buckling in particular. The panels are then stored for a couple of days at  $23^\circ\text{C}$  and 50% relative humidity which is a standard procedure before testing. The distance from the panel to the lenses is approximately 1120 mm and the distance between the lenses 218 mm. This arrangement of the setup equipment gives a picture size of 171x171 mm. The first step in calibrating the system is to align the cameras, figure 5.6, so that they are parallel and cover exactly the same area. This is done with help of the calibration program, see figure 5.7, which compares the images in real time and tells the user when the system setup is correct. Then a photo is taken and the cameras are moved, e.g. 4 mm backwards ( $z$ -direction). Then another photo is taken and the computer calculates the calibration parameters.

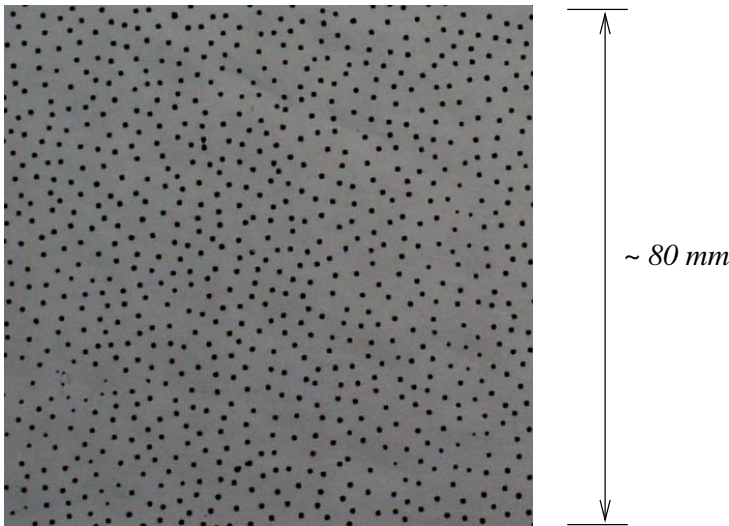


Figure 5.5: Photo of the speckle pattern.

The system is now calibrated and this is verified by performing a rigid body motion of 2 mm in the  $z$ -direction. The mean out-of-plane displacement from this test was  $2 \pm 0.02$  mm. Compare this value with the typical out-of-plane error of  $23 \mu\text{m}$ .

The MTS can register load and in-plane displacement of the movable crosshead versus time and because there is no connection to the DSP the synchronization has to be made by hand. The MTS is set up to compress the panel with a speed of 1 mm per minute and to register the load every 0.2 second. Thus, the test session can be summarized as:

1. Take a photo of the unloaded panel.
2. Start to compress the panel with a speed of 1 mm per minute.
3. When the load reaches 200 N, start to take a photo every 2 seconds until the panel breaks.
4. Let the computer calculate the 3D shape of the panel for each pair of photos and then the displacements from the difference in 3D shapes<sup>1</sup>.
5. Extract the load for every 2 seconds starting at 200 N.

---

<sup>1</sup>The cross correlation takes approximately 1 minute for each pair of photos on a SGI 540 (2x550 MHz Pentium III Xeon, 1 Gb Ram)

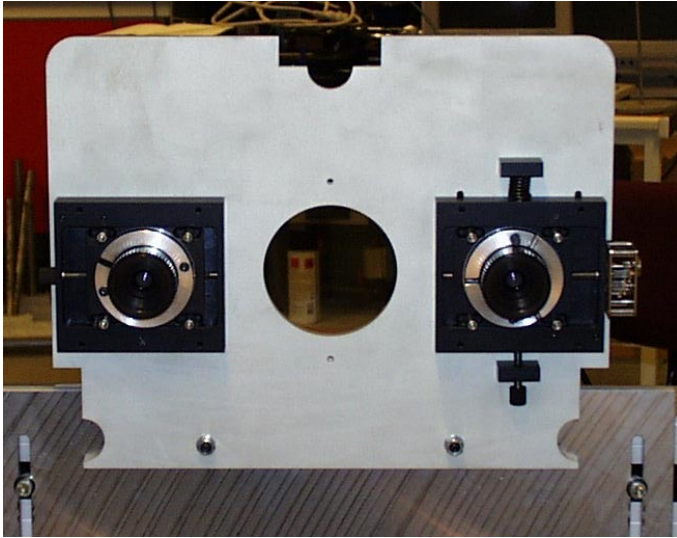


Figure 5.6: The camera to the left can be rotated and adjusted in the horizontal direction. The camera to the right can be adjusted in both the horizontal and the vertical direction.

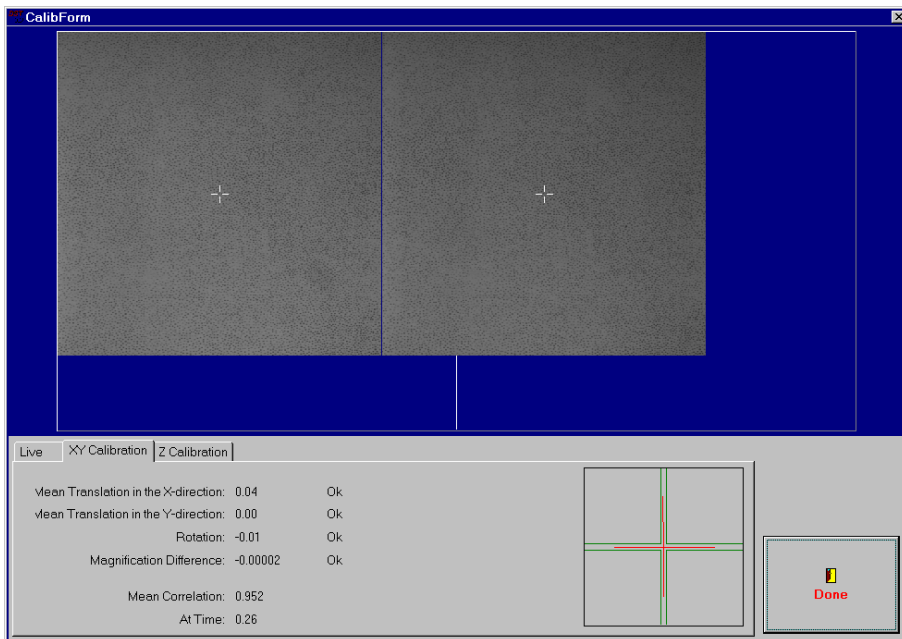


Figure 5.7: Screen-dump of calibration tool for the DSP.

Because that the edges are not perfectly straight they will be crushed until the force can be distributed over the whole edge. This behaviour varies a lot between the samples and that is the reason why no photos are taken before the load has reached 200 N.

## 5.3 Results

Seven tests were performed successfully and the load-displacement responses are seen in figure 5.8. Since the mid point of the test panel was not include in the area that the CCD-cameras covered, this value had to be calculated by extrapolation. This in order to be able to compare with the load-deformation curves from the FEA. The average peak load is 1677 N and the standard deviation is 2.6 % which is to be considered as a low value.

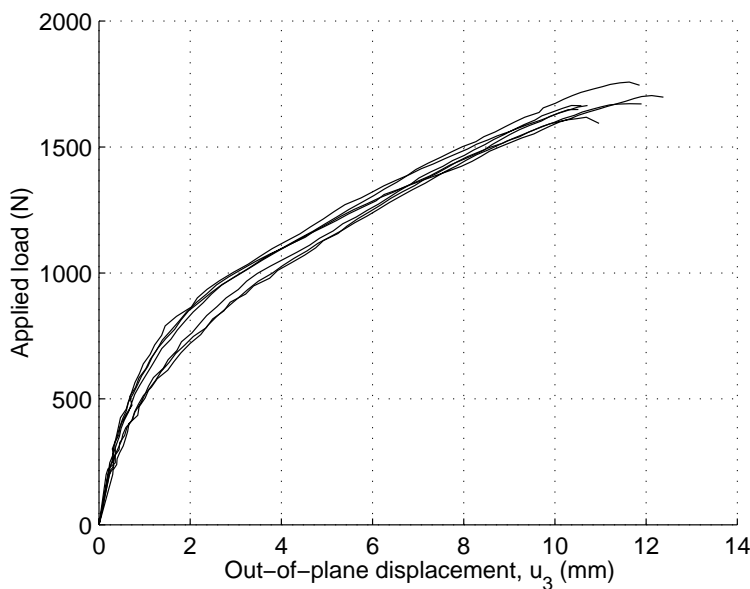


Figure 5.8: Load vs. displacement from experimental tests.

The shape of the cross sections in figure 5.9 shows that the panel can be considered to be simply supported. Although, the shape of the panel is not perfect symmetric as in the FEA.

As mentioned in section 5.2 was a smaller area studied in order to obtain a

Table 5.1: Results from experimental tests.

	Peak load (N)	Number of photos
Test 1	1758	63
Test 2	1618	57
Test 3	1705	65
Test 4	1673	63
Test 5	1668	66
Test 6	1665	59
Test 7	1651	59
Mean	1677	
Std. Deviation	44.2	
Std. Dev./Mean	0.026	

local buckling pattern. In the colour plots of the results, no such pattern could be found, due to the much larger global deformation. However, the local buckles could clearly be seen during the tests. To filtrate the global deformation, in the same way as it was done in the results from the FEA, was in this case not possible, since the exact locations of the output points were not known. Instead a photo was taken on the area where local buckling occurs, see figure 5.10. A photo of the most common collapse pattern was also taken, see figure 5.11. The global deformation pattern of the test panel, obtained from evaluation of the output results from the DSP-program, is seen in figure 5.12.

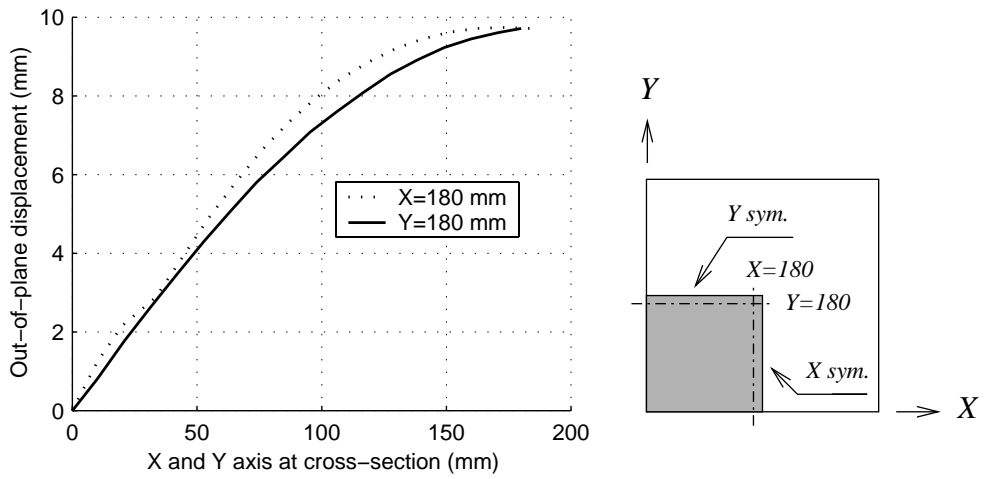


Figure 5.9: Shape along lines  $X=180$  and  $Y=180$  mm. Load  $\approx 1600$  N.

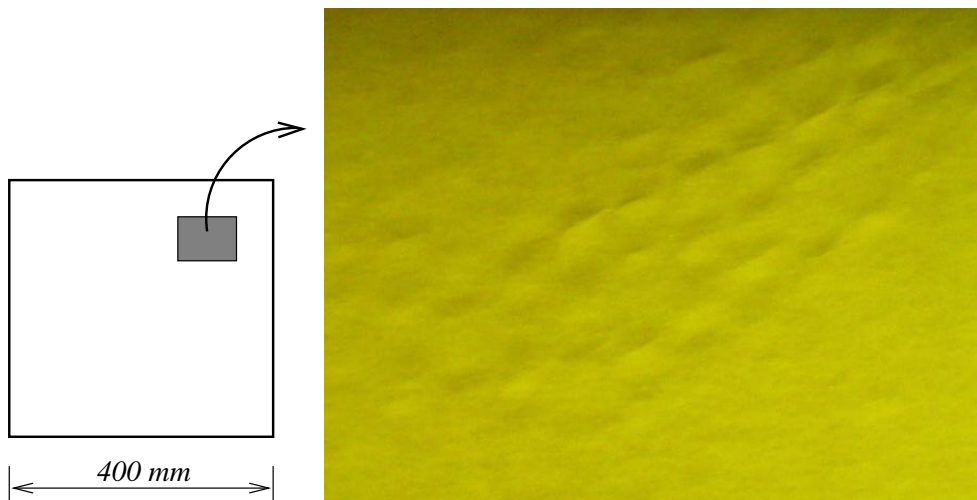


Figure 5.10: Photo of local buckling.

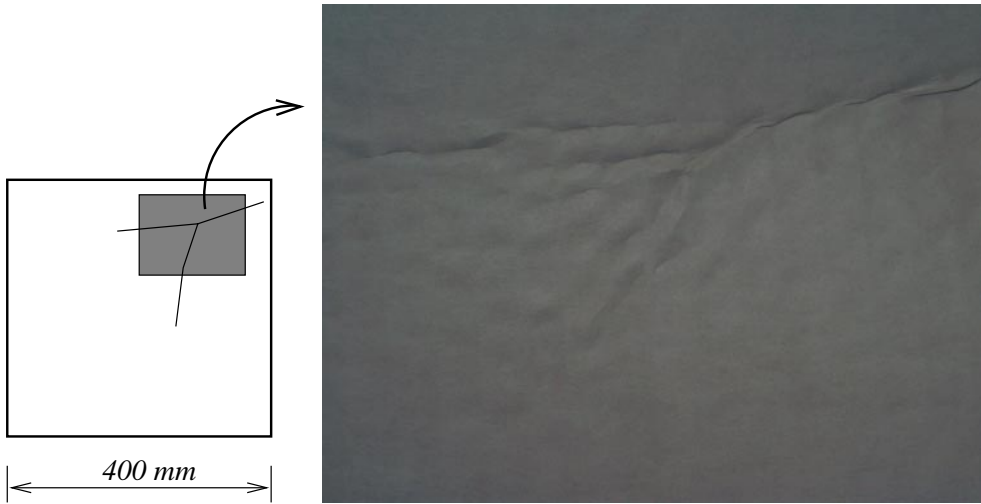


Figure 5.11: Photo of collapse pattern.

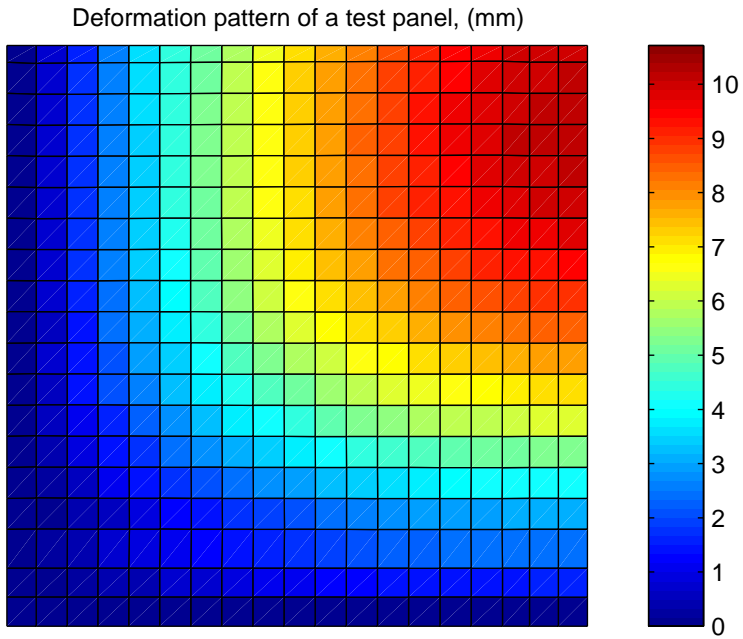


Figure 5.12: Global deformation pattern of a test panel.

# Chapter 6

## Comparison of results

In this chapter, the results from the FEA of the detailed and the simplified model No. 2 and the experimental tests are compared and the similarities and dissimilarities are discussed.

### 6.1 Load-displacement response

The load-displacement paths from the FEA<sup>1</sup> follows the ones from the experimental tests quite well as seen in figure 6.1. The initial stiffness is overestimated, but this is normal in a FEA of a perfect panel. Furthermore, it is reasonable that the panel loses stiffness during the beginning of the analysis when the edge is compressed. The load-displacement curves from the FEA that are presented in figure 6.1 do both have the No. 2 material parameters. These parameters gave the results that was most similar to the tests both considering the shape of the load-displacement curves and the location of where failure occurs.

A comparison of the section shape at cross section  $Y = 180$  mm between the FEA and the tests, see figure 6.2, shows that both the detailed and the simplified model have section shapes very similar to the tests. The cross section where  $Y = 180$  mm is chosen because in this section, no extrapolation of the out-of-plane displacement is done for the test. The somewhat larger out-of-plane displacement for the simplified model com-

---

<sup>1</sup>Due to the large amount of disc space used, the simulations were halted closely after the first point of local buckling (singular point, see section 4.6.1).

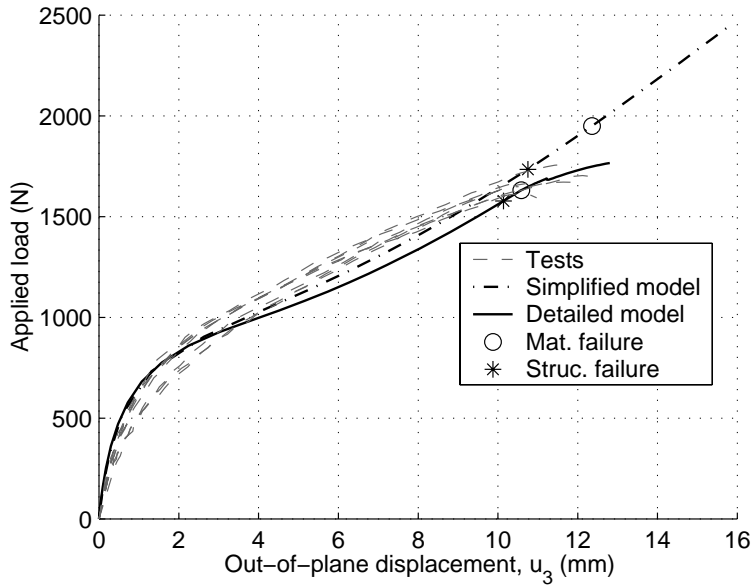


Figure 6.1: Load vs. out-of-plane displacement for experimental tests and the detailed and simplified models with the No. 2 material parameters.

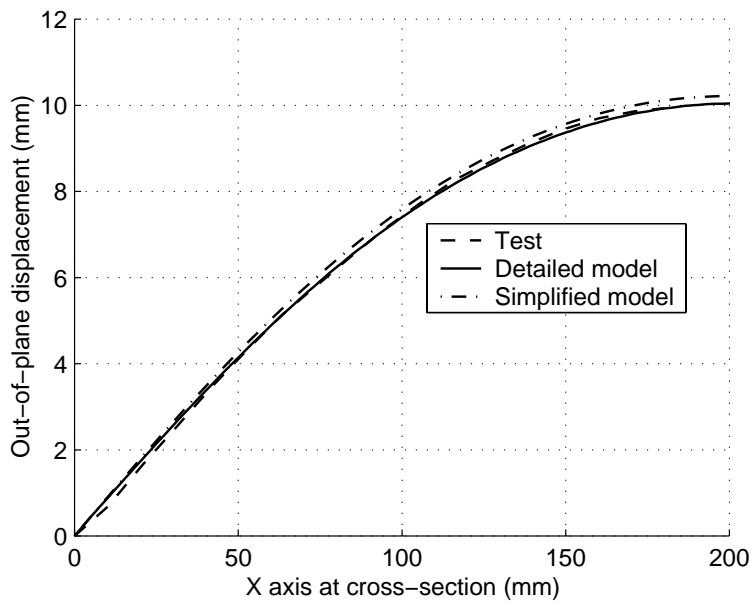


Figure 6.2: Comparison of shape along line  $Y=180$  mm for detailed and simplified model No. 2 and Test 3.

pared to the detailed, is a consequence of the large increment lengths that the analysis of the simplified model was performed in.

## 6.2 Stress development

In figure 6.3 it is shown how the stress levels changes with increasing out-of-plane displacement at two points, A and B, for the detailed and the simplified model. These points are both situated on the outer side of liner 200 WTK, on which the local buckling will occur. At point B the stress levels for the two models do not differ very much. For  $\sigma_{11}$  a small tendency of divergence of the two models can be seen, at an out-of-plane displacement of approximately 11 mm. Otherwise, the behaviour of the detailed and the simplified model is quite similar at this point. At point A, the stresses follows each other fairly until a certain point is reached. From this point the stress-displacement curves for the detailed model diverge from the prior shared path. The point where this occur corresponds well to the point where local buckling first can be observed. The stress levels for the detailed model then becomes substantially higher than for the simplified model, at the same out-of-plane displacement.

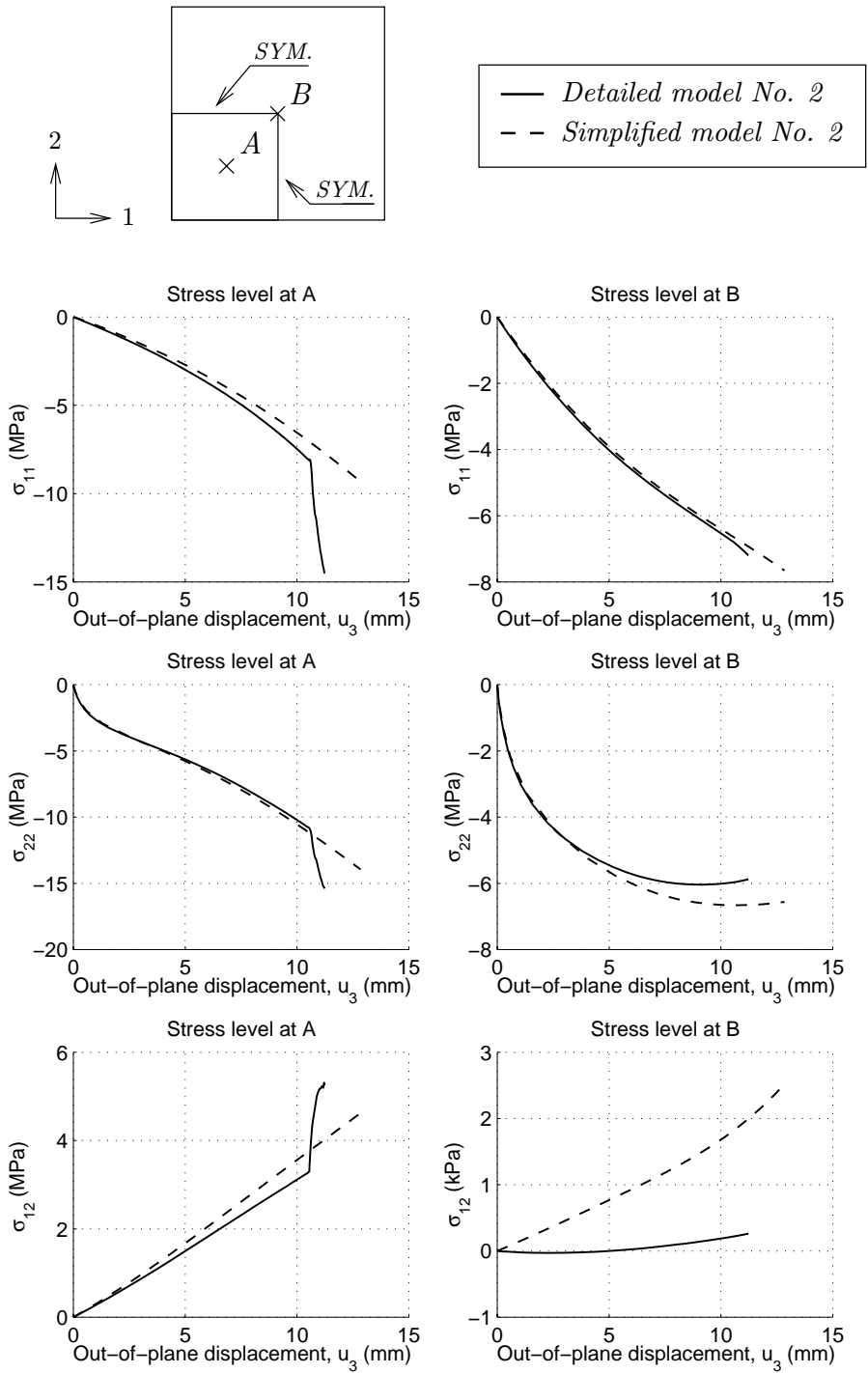


Figure 6.3: Stress vs. out-of-plane deformation for detailed and simplified model No. 2. Liner 200 WTK

## 6.3 Failure criteria

In figure 6.4 and 6.5, the structural failure index is presented for the detailed and simplified model respectively. The load level, when structural failure is initiated, is for the detailed model 1580 N, 5.8 % less than the mean peak load for the tests, 1677 N, and for the simplified model 1730 N, which is 3.2 % larger than the tests mean value. Thus, both of the models yields reasonable values of the load level when failure occurs.

An investigation of where the structural failure index has the largest value, showed that this place is almost identical for the detailed and the simplified model, namely on the upper symmetry boundary, close to the centre. However, from the tests it was observed that the region where collapse, i.e. material failure, was initiated, was situated closer to the corner. If instead the Tsai-Wu criterion for the detailed and the simplified model is examined, see figure 6.6 and 6.7, the locations, where the failure index exceeds 1.0, corresponds more accurate to the tests. For the detailed model the largest value of the Tsai-Wu criterion is situated in the area where local buckling occurs. For the simplified model this point is situated closer to the corner of the plate.

The load level for the detailed model, when the material failure index exceeds 1.0, is 1630 N. This is less than 3 % lower than the mean value of the peak load for the tests, 1677 N. For the simplified model, the load level when the material failure index exceeds 1.0, is 1950 N. This is 16.3 % larger than the mean value of the tests. This shows that the local buckling phenomena has an influence, at which load level material failure is initiated. Thus, a detailed model which in detail models the fluting, is needed to accurately get a value of the load level when material failure first occurs.

Table 6.1: Comparison of the load level at failure between the experimental tests and the FEA of the detailed and simplified model No. 2.

	Exp. tests	Detailed model		Simplified model	
Struc. fail. (N)	1677	1580	-5.8 %	1730	+3.2 %
Mat. fail. (N)	1677	1630	-2.8 %	1950	+16.3 %

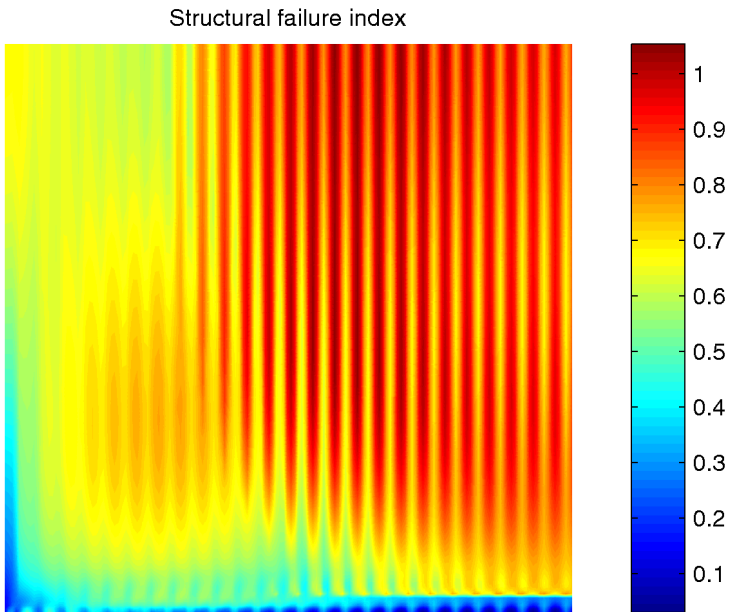


Figure 6.4: Structural failure criterion for the detailed model No. 2. Load = 1580 N. Out-of-plane displacement = 10.1 mm. Liner 200 WTK.

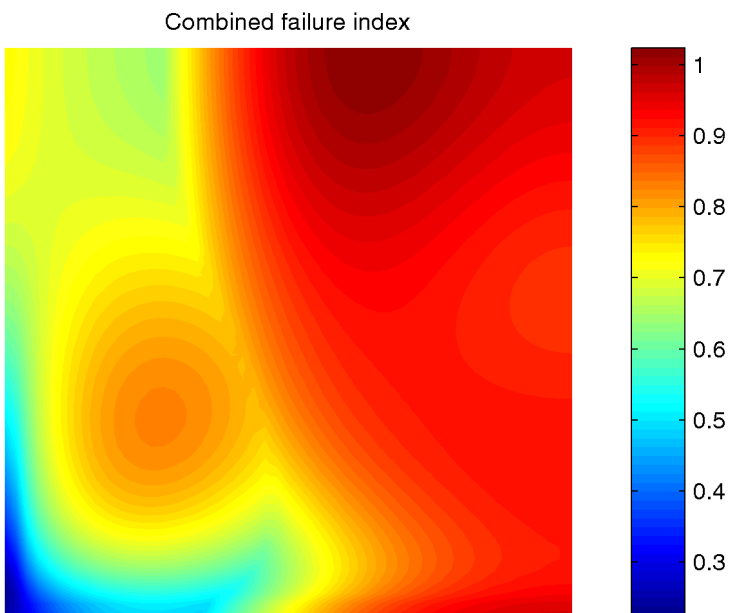


Figure 6.5: Structural failure criterion for the simplified model No. 2. Load = 1730 N. Out-of-plane displacement = 10.7 mm. Liner 200 WTK.

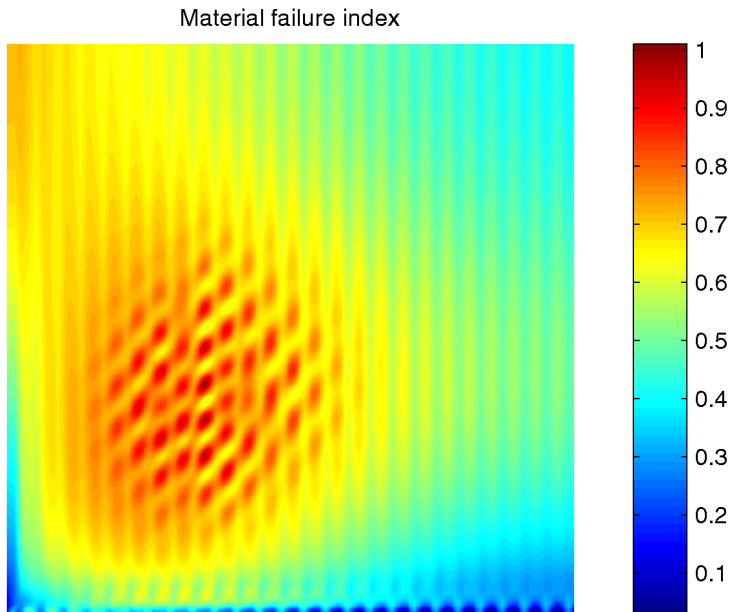


Figure 6.6: Material failure criterion for the detailed model No. 2. Load = 1630 N. Out-of-plane displacement = 10.6 mm. Liner 200 WTK.

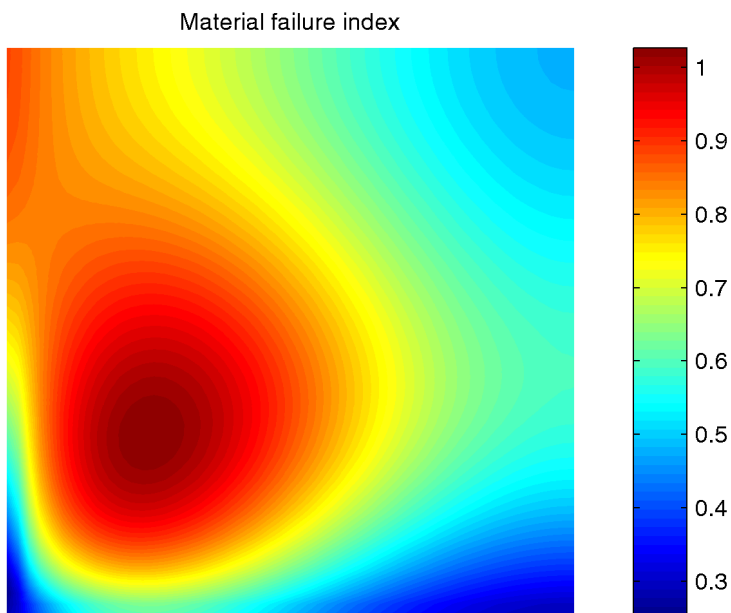


Figure 6.7: Material failure criterion for the simplified model No. 2. Load = 1950 N. Out-of-plane displacement = 12 mm. Liner 200 WTK.



# Chapter 7

## Concluding remarks

### 7.1 Conclusions

The agreement of the load-displacement responses are good even when a linear-elastic material model is used. With the use of a failure criterion that takes both material and structural failure in account, the collapse load can be estimated with acceptable accuracy both for the detailed and the simplified model.

Choosing the material parameters is not easy. They can be chosen within a wide range and be reasonable, but still the result from the FEA may differ somewhat from the experimental test. The out-of-plane shear moduli,  $G_{xz}$  and  $G_{yz}$ , are of great importance for the magnitude of the local buckling load.

### 7.2 Future work and improvements

The most important improvement could be to introduce an orthotropic material model that incorporates plasticity. This would prevent the stiffness from increasing after buckling. Another area could be the connection between the liner and fluting. In this analysis, the connection is modelled as a rigid coupling and this makes the stiffness of the structure overestimated.

The introduction of local perturbations could also decrease the initial

tangential stiffness, so that the load-displacement paths are in better agreement before the first bifurcation point.

Instead of using the global load for comparison between the FEA and experiments, a better response measure would be the local strains at collapse compared to calculated strains. This requires calculations of gradients of the measured displacements, since the only output from the DSP is the displacements.

# Bibliography

- [1] Grafiska yrkesnämnden, (1985), *Wellpapp - Grundkurs*, Stockholm
- [2] Svenska Wellpappföreningen, <http://www.swif2000.com>
- [3] SCA Packaging, *Boxing*
- [4] Stiftelsen Packforsk, <http://www.packforsk.se>
- [5] Persson, K., (1991), *Material Model for Paper: Experimental and Theoretical Aspects*, Diploma Report, Lund University, Sweden
- [6] Mann, R.W., Baum, G.A. and Habeger, C.C., (1980), *Determination of all nine orthotropic elastic constants for machine-made paper*, Tappi, Vol. 63, No. 2, pp 163-166
- [7] Baum, G.A., Brennan, D.C. and Habeger, C.C., (1981), *Orthotropic elastic constants of paper*, Tappi, Vol. 64, No. 8, pp 97-101
- [8] Hibbit, Karlsson & Sorensen Inc., *ABAQUS/Standard Version 5.8*, Pawtucket, RI
- [9] Tsai, S.W. and Wu, E.M., (1971), *A General Theory of Strength for Anisotropic Materials*, J. Comp. Mater., **5**, pp 58-80.
- [10] Fellers, C., Westerlind, B. and de Ruvo, A., (1983), *An Investigation of the Biaxial Failure Envelope of Paper: Experimental Study and Theoretical Analysis*. In Transaction of the Symposium, Cambridge, Vol. 1, pp. 527-559
- [11] Gustafsson, P.J., Nyman, U. and Heyden, S., *A Network Mechanics Failure Criterion*. Report TVSM-7128, Division of Structural Mechanics, Lund University

- [12] Nyman, U. and Gustafsson, P.J., *Material and Structural Failure Criterion of Corrugate Board Facings*, Composite Structures, Accepted for publication
- [13] Nyman, U. and Gustafsson, P.J., (1999), *Local Buckling of Corrugated Board Facings*. Proceedings of the European Conference on Computational Mechanics, Munich, Germany
- [14] Nordstrand, T.M., (1995), *Parametric study of the post-buckling strength of structural core sandwich panels*, Composite Structures, **30**, pp 441-451
- [15] Timoshenko, S. P. and Gere, J. M., (1961), *Theory of Elastic Stability*, McGraw-Hill
- [16] Nyman, U. and Gustafsson, P.J., *Buckling of Long Orthotropic Plates Including High-Order Transverse Shear*. Submitted to J. of Engineering Mechanics
- [17] Patel, P., (1996), *Biaxial Failure of Corrugated Board*, KFS AB
- [18] Magnusson, A., (2000), *Branch Identification In Elastic Stability Analysis*, Doctoral Thesis, Division of Solid Mechanics, Lund University
- [19] Sjö Dahl, M., (1995), *Electronic Speckle Photography applied to In-plane Deformation and Strain Field Measurements*, Doctoral Thesis 1995:171 D, Luleå University of Technology, Division of Experimental Mechanics
- [20] Synnergren, P., (1996), *Stereo-ESP, optiskt mätsystem för bestämning av tredimensionella förskjutningsfält och form*, Master Thesis 1996:008 E, Luleå University of Technology, Division of Experimental Mechanics
- [21] Synnergren, P., (1998), *Stereoscopic Digital Speckle Photography*, Licentiate Thesis 1998:23, Luleå University of Technology, Division of Experimental Mechanics